Aalto-yliopisto
Aalto-universitetet
Aalto University

Master’s Programme in Mechanical Engineering

Experimentally based surrogate models for volumetric compressibility of partially saturated bentonite clay

Samuel Forsman

Master’s thesis
2024

Aalto-yliopisto
Aalto-universitetet
Aalto University

Author Samuel Forsman

Title of thesis Experimentally based surrogate models for volumetric compressibility of partially saturated bentonite clay

Programme Master's Programme in Mechanical Engineering

Major Mechanical Engineering

Thesis supervisor Prof. Sven Bossuyt

Thesis advisor(s) D.Sc. Veli-Matti Pulkkanen

Collaborative partner VTT

Date 05.09.2024 **Number of pages** 78 **Language** English

Abstract

The thesis objective was to develop experimentally based surrogate models for volumetric compressibility of partially saturated bentonite clay. Bentonite is a natural swelling clay used in several geotechnical applications. This thesis focuses on bentonite's role in the multi-barrier concept for the final disposal of nuclear waste in deep geological repositories. Developing experimentally based surrogate models for bentonite's elastic and plastic behaviour can increase understanding of the relationship between critical factors affecting bentonite's mechanical behaviour.

A literature review provides the reader with a clear description of the relevant concepts and the current state of bentonite barriers in the final disposal concept. After the Literature Review, a new independent compaction station for volumetric compaction is developed and tested. After that, the researcher carefully drafts the design of experiments, which includes four main conditions: bentonite type, water content, water salinity and waiting time. Mechanical compactions are conducted according to the design of experiments in the new independent compaction station. The compaction data are examined, and the elastic and plastic hardening parameters are obtained from the calibrated data by using the elastoplastic models presented in the Literature Review. The hardening parameters are used to develop the elastic and plastic surrogate models separately.

The elastic surrogate model identifies bentonite type as the most significant factor, where sodium bentonite is more resistant to elastic deformations than calcium bentonite. The water salinity mix that matches the realistic environment in the bedrock increased resistance in the elastic model. Water content and waiting time did not significantly impact the model. Similarly, the plastic surrogate model's most significant factor was the bentonite type. However, calcium bentonite will be more resistant towards plastic deformations than sodium bentonite. The remaining factors were consistent with the findings of the elastic model. These findings explain the relationship between critical factors and serve as a robust framework for predicting bentonite's mechanical behaviour.

Keywords bentonite, surrogate models, design of experiments, compaction

Table of contents

Preface and Acknowledgements

I am grateful to the following individuals for their unwavering assistance and support throughout my work on this thesis and my years at Aalto University:

- *Veli-Matti Pulkkanen* for his expertise, knowledge, and guidance during my time at VTT.
- *Sven Bossuyt* for his support as my thesis supervisor.
- *Olli-Pekka Rauhala, Anniina Seppälä, Sharma Mrityunjai, Pirjo Hellä, and Emmi Myllykylä* for their insights and support in helping me make informed decisions throughout this journey.
- *Hannu Vesala, Pekka Sinkkonen, and Kirsti Helosuo* for guiding and helping me in the laboratory.
- *My fellow students* for their camaraderie, encouragement, and support throughout my years at Aalto University.
- *My friends and family* for their unwavering support, love, and encouragement.

Symbols and Abbreviations

Symbols

p	Pressure
V	Volume
σ_{ij}	Stress Tensor Components
ε_{ij}	Strain Tensor Components
κ	Elastic Compressibility Parameter (Kappa Value)
λ	Plastic Compressibility Parameter (Lambda Value)
e	Void Ratio
φ	Porosity
ρ	Density
ρ_{dry}	Dry Density
w	Water Content
ε_V	Volumetric Strain
p	Mean Stress
v	Poisson's Ratio
E	Young's Modulus

Abbreviations

DoE	Design of Experiments
IPCC	International Panel on Climate Change
IEA	International Energy Agency
NCL	Normal Compression Line
R^2	Coefficient of Determination
Q^2	Predictive Power of the Model
TDS	Total Dissolved Solids
VTT	Technical Research Centre of Finland (Valtion Teknillinen Tutkimuskeskus)

1 Introduction

In this chapter, the background and the objectives for the thesis are presented.

1.1 Background

In the International Panel on Climate Change's (IPCC) latest report from 2023, a warning was issued stating, *"Human activities, principally through emissions of greenhouse gases, have unequivocally caused global warming"*. The increase in the emission of greenhouse gasses has resulted in extensive adverse effects, causing losses and harm to both the environment and human beings (Lee et al., 2023). A significant contributor to the increase in greenhouse gas emissions is using fossil fuels for energy production, accounting for 81% of the energy produced in 2023 (EI, 2024). To address this pressing issue, it is essential to reduce global greenhouse gas emissions by 2030 drastically (Horowitz, 2016). This has prompted the search for renewable alternatives for energy production.

While wind and solar power will lead the way towards replacing fossil fuels, nuclear energy will serve as a complementary energy resource to further reduce the dependency on fossil fuels. Currently, nuclear energy is the second largest source of low-emission power, following hydropower (Peter Fraser, 2022). In 2021, 33% of the total electricity generation in Finland was produced from nuclear energy, and with the completion of Olkiluoto 3 in 2023, this number is expected to increase to 40%. The increase in electricity generation from nuclear energy plays a vital role in the Finnish government's plan to achieve carbon neutrality in 2035, as well as making Finland less dependent on energy imports from other countries (IEA, 2023).

During the operation of a nuclear power plant, uranium is used as the primary fuel for electricity production. Post-use, the uranium remains highly radioactive, posing potential hazards to both humans and the environment if not handled properly. Therefore, safe nuclear waste management is mandatory to successfully operate a nuclear power plant. According to the Nuclear Energy Act, it is required that all nuclear waste generated in Finland must be stored and disposed of in Finland. The act further mentions that the producers of nuclear waste are also responsible for all associated costs as well as the necessary nuclear waste management activities (IEA, 2023).

In 2000, the Finnish government decided to examine variations for the final disposal of nuclear waste and deemed deep geological sites most promising. Their motivation read like this: *"Out of the investigated final disposal* *options, final disposal deep in bedrock, i.e., geological final disposal, offers the best and most realistic possibilities to isolate high-level nuclear waste from the biosphere, i.e., the human habitat"* (Kontula et al., 2021). In 2015, the Finnish government granted Posiva, a jointly owned company by the two nuclear power operators in Finland, a construction license to build Onkalo close to the Olkiluoto nuclear power plant (IEA, 2023).

Onkalo started as the test facility for the final disposal site of spent nuclear fuel in Olkiluoto but now serves as the final disposal facility as well. The spent nuclear fuel is put into airtight double-layered metal canisters and then brought down 400 meters underground into crystalline Finnish bedrock. Tunnels in the bedrock are excavated, and holes are drilled in the tunnels, which are 10 meters between each hole. A bentonite buffer is then placed in the holes. The metal canister with the nuclear waste contents is placed inside the bentonite buffer. Lastly, to close the holes, bentonite blocks are placed on top of the canister, and the tunnels are backfilled (IEA, 2023; Posiva Oy, 2013; Vehmas et al., 2023). **Figure 1** shows a visual representation of the final disposal of nuclear waste in deep geological sites.

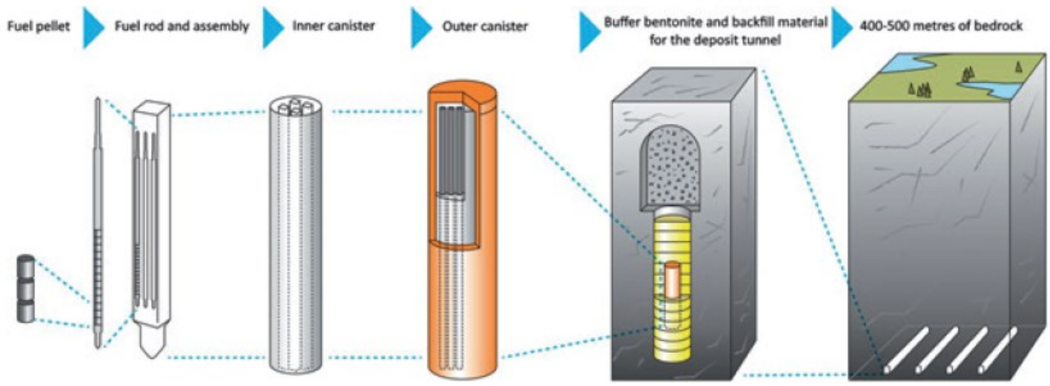

Figure 1: Posiva's multi-barrier solution for final disposal of nuclear waste (Vehmas et al., 2023).

The bentonite barriers serve as one of the three critical components in the multi-barrier system, protecting the nuclear waste along with the metal canisters and the bedrock granite (Vehmas et al., 2023). The design of the bentonite buffer blocks is divided into three layers: the outer ring block, the inner ring block, and the centre block. The outer and inner ring blocks are segments of a circle, while the center block is the shape of a cylinder (Muuri, 2021). The block segments are visually represented in **Figure 2**.

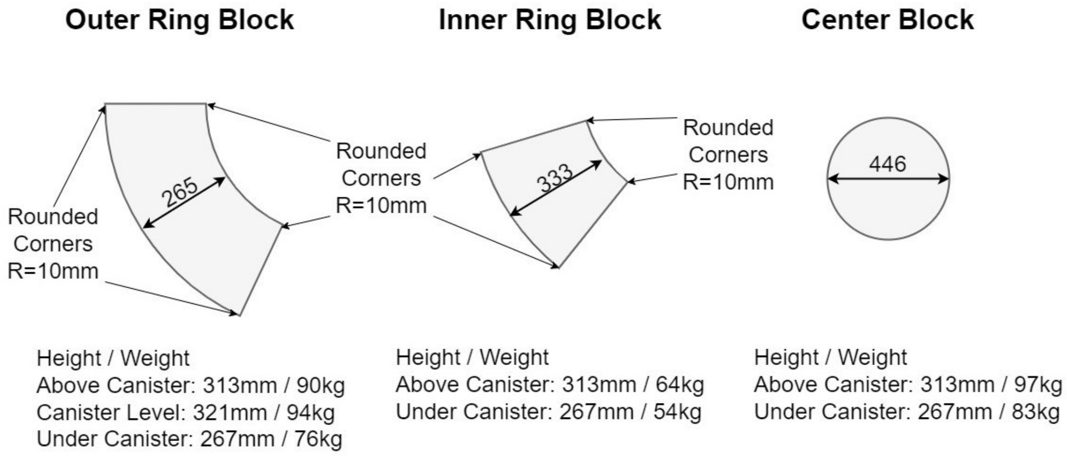

Figure 2: The design of the bentonite blocks used in deep geological disposal sites with its measurements (Muuri, 2021).

The bentonite blocks are placed below, around, and above the metal canisters. The outer and inner ring blocks are arranged to form a complete circle, which is then sealed with the center block. Pellets are also placed between the metal canister and the inner ring blocks and between the outer ring blocks and the bedrock. To enable the placement of the segment blocks, a chamfered block is placed at the top of the hole (Muuri, 2021) according to **Figure 3.**

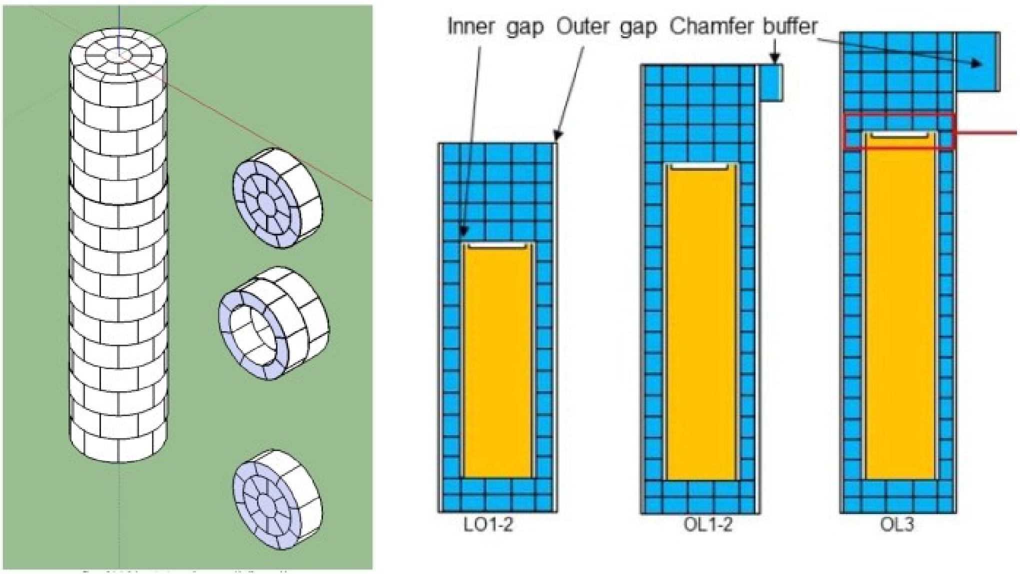

Figure 3: The placement of the bentonite blocks in the deposition holes (Muuri, 2021).

This overview highlights the critical role of bentonite buffers in ensuring the long-term safety and stability of the final geological disposal concept. Transitioning from this overview, the next chapter delves into the details of the old compaction station used for compacting and examining bentonite samples at VTT.

1.1.1 Volumetric Isotropic Compaction with Triaxial Test Station

The bentonite buffers play a vital role in the multi-barrier solution for the final disposal of nuclear waste. Simultaneously, the bentonite buffers need to meet all necessary safety functions, which are met by fulfilling all performance targets and design requirements listed in Chapter 2. The safety functions regulate the design parameters of the bentonite buffer, which consequently impacts the mechanical properties of the barrier. The mechanical behaviour of the bentonite barrier is a well-established research problem, and extensive research has been done on the subject. However, there is still a need to further the understanding of the mechanical behaviour and test the barriers in unexplored configurations. With this need for a proper understanding of the barrier's mechanical behaviour, a reliable and accurate method to produce the samples for testing is also needed.

Bentonite is a soil material which can undergo volumetric plastic deformation and whose shearing behaviour depends on the hydrostatic stress. Therefore, comprehensive testing through volumetric compression and triaxial tests is required to assess bentonite's mechanical behaviour. These tests are essential for understanding the bentonite's elastoplastic stress-strain relationship and other critical mechanical characteristics under various conditions. To avoid anisotropy, the samples used in the triaxial tests should be produced from isotropic compaction. To this end, to produce the samples, bentonite grains are placed under isostatic pressure until the final form of the samples is obtained. Meanwhile, the volume change is measured to obtain data of the volumetric compression.

Previously, the bentonite samples have been volumetrically compacted in a triaxial shear test apparatus from GDS Instruments, seen in **Figure 4**. The device consists of a cell where the bentonite sample will be placed and a vertical load arm to put an axial strain on the sample. The pressurised fluid used in this apparatus is silicon oil. This setup allows for precise control of sample's shear and hydrostatic pressure components of stress that allows following complicated stress paths in the mechanical experiments. However, the existing triaxial test apparatus is not ideal for producing isotropic compacted bentonite samples.

While the apparatus is versatile and capable of compacting and conducting shear tests on bentonite samples, it has shortcomings in volumetric compaction. Firstly, having the same apparatus doing volumetric compaction and triaxial shearing will keep the apparatus occupied constantly and vulnerable to breakdowns. Secondly, the silicon oil used as the pressurised fluid is messy, and other fluids could be at least equally good for volumetric compaction of samples but not as messy. Lastly, the GDS Instruments apparatus can only compact samples up to 32MPa. A device able to compact bentonite samples to a higher maximum pressure is needed to enable producing samples with high water content and dry density that correspond the bentonite conditions in the deep geological disposal sites.

Figure 4: The triaxial shear test apparatus from GDS Instruments used for compacting bentonite sample.

These challenges and shortcomings highlight the need for a second dedicated volumetric compaction device. This second device would be able to handle all volumetric compaction of bentonite samples independently, allowing the triaxial cell to be reserved for shear testing only. This clear division of functions would improve availability and enhance the experimental results' reliability and accuracy.

1.2 Objectives of the Thesis

Even though Finland has one of the highest public support for nuclear energy, with 60% of the people having a positive stance towards it (IEA, 2023), there is potential to increase this support even further. Informing and improving public understanding of the final disposal concept and further developing this concept play a crucial role in achieving this. The bentonite buffers are one vital part of the final disposal concept, and by fully understanding bentonite's mechanical behaviour, optimised solutions to the bentonite buffer can be found.

The main objective of this thesis is to produce experimentally based surrogate models for elastic and plastic volumetric compression model parameters. This goal is driven by the need for accurate and reliable models to predict the mechanical behaviour of bentonite buffers under various configurations, which is critical for its application in the final disposal concept. To achieve this primary objective, several interim objectives have been established, each contributing to the overall success of the research. The interim objectives are:

- Conduct background research.
- Develop a volumetric compaction system that is easier and more reliable.
- Determine material and conditions.
- Minimize the needed number of samples with Design of Experiments (DoE).
- Conduct mechanical tests according to DoE.
- Test and fit mechanical constitutive models.
- Surrogate Model Fitting.
- Determine the most important effects.

The research aims to develop accurate surrogate models for predicting bentonite's elastic and plastic behaviour by systematically addressing the interim objectives. These models will be instrumental in advancing the knowledge about bentonite buffers in the final disposal concept.

1.3 Research Approach

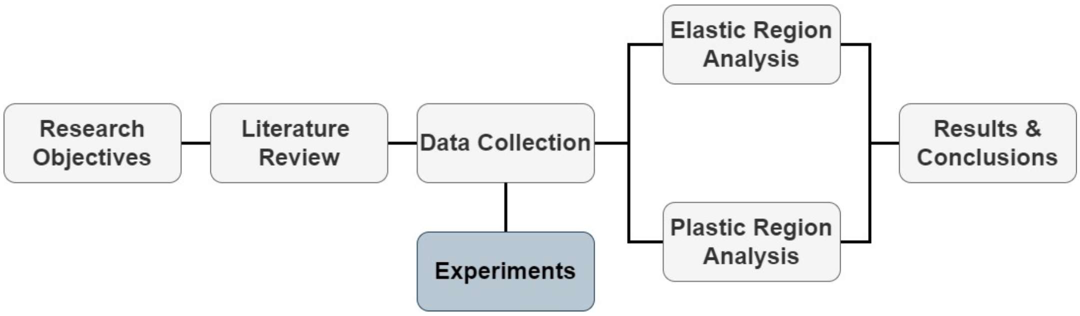

Figure 5: Research process flow chart.

This study follows the research process illustrated in **Figure 5**. Firstly, a clear and focused main objective was defined for the study, along with interim objectives. The second step involved conducting a literature review to gain a deeper understanding of the topic before starting data collection. Data was collected from a carefully drafted Design of Experiments (DoE). An analysis of the data was conducted, with a focus on analysing the elastic regions and plastic regions separately. Finally, conclusions were drawn based on the findings and the results.

Bell et al. (2019) outline qualitative and quantitative research strategies as the main approaches. *Qualitative* research interprets social reality by analysing non-numerical data, such as words and images. On the contrary, the *quantitative* research strategy focuses on quantifying data and using this data to answer research questions and test hypotheses through statistical analysis (Bell et al., 2019). Given this thesis's research objective, a quantitative research strategy approach was chosen.

Research design is a framework for how the collection of data and analysis of the data is conducted. Two common research design types are case study design and experimental design. A case study design is appropriate when a better understanding of a studied case wants to be achieved, and only that case is analysed. An experimental research design is a method to find cause-and-effect relationships between dependent and independent variables (Bell et al., 2019). This thesis takes an experimental design approach by carefully creating a DoE with varying variables and examining their effects.

In this thesis, a literature review was conducted to establish a solid foundation on the existing knowledge for its topic. Bell et al. (2019) define a literature review as gathering current knowledge about a research topic through various mediums. The literature review serves as the foundation for the researcher when approaching the research problem. A literature review can either be *systematic* or *narrative,* depending on how the researcher conducts the literature review (Bell et al., 2019).

A systematic approach to the literature review involves examining all existing literature for the research topic in a structured and repeatable manner. By following a systematic approach, the researcher can critically evaluate and systematically filter out studies and literature that are irrelevant to the research topic. In contrast, a narrative approach to the literature review allows the researcher to proceed iteratively and is not restricted to following any specific methodology. Therefore, the researcher can adapt to new directions and set new boundaries as the understanding of the literature evolves (Bell et al., 2019).

Since this study employs a quantitative research strategy, a systematic method for the literature review was chosen. This systematic approach was selected because bentonite barriers in the final disposal concept is a well-established research question, and many design factors and requirements already exist regarding what the bentonite barriers should achieve. The research was conducted through various platforms such as Google Scholar and Aalto Library, where scientific articles and books were thoroughly read and examined.

2 Literature Review

In Posiva's safety evaluation from 2016, 8 performance targets for the buffer in the final disposal concept for nuclear waste were listed. The performance targets apply to the long-term safety and behaviour of the final disposal concept. These eight performance targets are (Posiva Oy, 2016b):

- *The amount of substances in the buffer that could adversely affect the canister, filling components, compartment plugs, and drift plugs or host rock shall be limited.*
- *The buffer should have a sufficient swelling capacity.*
- *The buffer shall fulfil the requirements listed below over hundreds of thousands of years in the expected repository conditions.*
- *The buffer shall transfer the heat from the canister efficiently enough to keep the buffer temperature < 100 °C.*
- *The buffer shall allow gases to pass through it without causing damage to the repository system.*
- *The buffer shall limit microbial activity.*
- *The buffer shall be impermeable enough to limit the transport of radionuclides from the canisters into the bedrock.*

After that, six design requirements for the buffer are listed; the design requirement applies to the initial state of the bentonite buffer. The six design requirements are (Posiva Oy, 2016b):

- *The main component of the buffer material shall consist of natural swelling clays.*
- *The buffer shall be designed to be self-sealing after initial installation and self-healing after any hydraulic and mechanical disturbances.*
- *The buffer shall be so designed that the possibility of corrosion of a canister by sulphide and other corrodants, including microbially-induced processes, will be limited.*
- *The buffer shall be so designed that it will mitigate the mechanical impact of the postulated rock shear displacements on the canister to the level that the canister integrity is preserved.*
- *The buffer shall have sufficiently fine pore structure so that transport of radionuclides formed within or around the canister is limited.*

Bentonite was chosen as the buffer material because it effectively meets all the performance targets and design requirements for the final disposal concept's initial state and long-term safety and stability.

2.1 Bentonite

This chapter introduces the foundation for bentonite and the bentonite buffers, including the montmorillonite structure and the bentonite buffers' loads, design parameters and production process.

2.1.1 Montmorillonite

To fully comprehend the behaviour of bentonite, it is essential to review its origin and nanoscale properties. The formation process started several million years ago when volcanic glass interacted with freshwater or seawater with a low pH value. This interaction process will turn the volcanic glass into a type of clay called smectite. Smectites are a material group with a unique layer structure. Montmorillonite, a member of the smectite clay group, becomes the primary component of bentonite when the clay predominantly consists of montmorillonite (Haldar & Tišljar, 2014).

The montmorillonite structure is complex and comprises three layers, two SiO_4 tetrahedral layers, and one Al octahedral layer, bonded to each other. The outer tetrahedral layers carry a negative charge due to substituting Al and Mg atoms with the octahedral layer. This results in sandwich-like structures forming where positively charged cations and water molecules will occupy the interlayer spaces, as illustrated in **Figure 6**. The combined thickness of the tetrahedral layers and the octahedral layer is below 1 nm (Haldar & Tišljar, 2014; Pulkkanen, 2019).

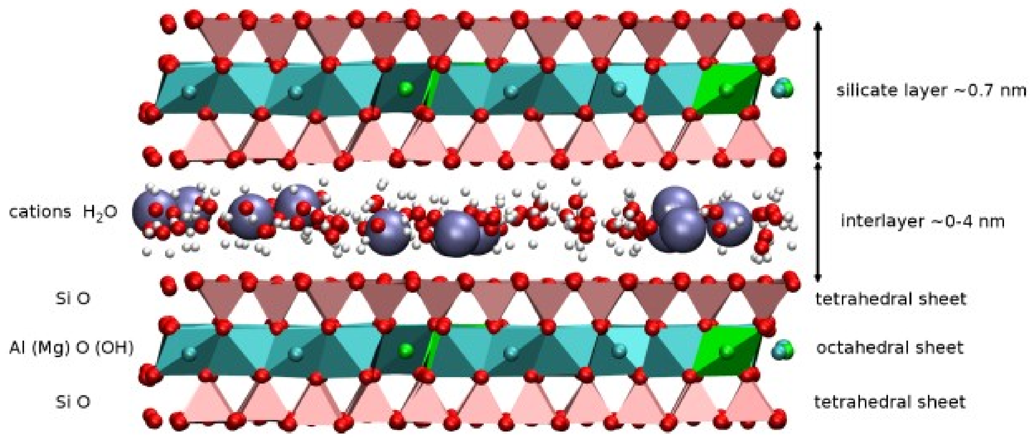

Figure 6: The montmorillonite structure and layers. The figure is from molecular dynamics simulations conducted by Anniina Seppälä.

Figure 6 illustrates an idealized version of the montmorillonite layer at the nanoscale. However, when going from nanoscale to larger scales, the layers might become intertwined. This will lead to imperfections, causing the layers to bend and lose uniformity. Therefore, with these imperfections in the real-scale layers of montmorillonite, the swelling of bentonite is not as straightforward as it is with just adding water in the interlayer sections (Pulkkanen, 2019).

Montmorillonite's complex layer structure is vital to understanding bentonite's mechanical behaviour. While on a nanoscale, montmorillonite appears organized, real-scale observations reveal complexities due to layer intertwining. These structural intricacies greatly influence the swelling and the overall mechanical properties of bentonite. Before delving into the design parameters crucial for buffer design, exploring the various loads impacting the bentonite buffer is essential. The subsequent section will dissect the four distinct loads influencing the buffer within the final disposal concept.

2.1.2 Bentonite Barrier Loads

Four different loads acting on the bentonite barriers in the final disposal concept of nuclear waste can be identified. The four different loads are mechanical loads, chemical loads, thermal loads, and radionuclide loads (Juvankoski, 2013). The specific loads will create individual challenges for the bentonite barriers; thus, the loads need to be examined and understood.

Mechanical loads are the loads created from the buffers' weight and pressure. Also included in the mechanical loads are the external mechanical loads acting on the buffer, which originate from the natural environment, the weight of the canister, and the tunnel backfilling. Sudden rock shear displacements are also taken into consideration when examining mechanical loads. These sudden movements are what dictate the highest allowed buffer density. Additionally, as wetting of the bentonite barrier takes place gradually over time, swelling of the barrier will occur and cause stress changes in the buffer and towards the canister. Several studies have experimented with different compression pressures, densities, and weights. The conclusion that could be drawn from these studies was that over the expected lifespan of 100,000 years, the anticipated movement of the canister within a deposition hole due to consolidation and creep is minimal. In fact, with a relatively soft backfill, it may even lead to a slight upward movement of the canister (Juvankoski, 2013).

Chemical loads affecting the buffer originate from the environment around the buffer. The chemical loads from different groundwater compositions will affect bentonite's behaviour. Five main risks from external chemical loads can be identified. The first risk is that the salinity of the absorbed water will affect the swelling of the bentonite. The second risk is that with a too-high cation concentration, a loss of buffer mass could occur due to erosion. Thirdly, buffer swelling pressure may be lost if the pH of the absorbed water is too high. Fourthly, chlorination of the buffer may happen if the concentration of iron is too high (Juvankoski, 2013). Lastly, erosion due to dilute water intrusion to disposal depth may occur.

Thermal loads on the buffer are generated due to decay heat from the canisters with the spent nuclear fuel contents. The thermal conductivity in the early stages of the buffer installation is relatively low because the buffer blocks are still dry. After a long time, the buffer will become saturated and homogenized, thus increasing the thermal conductivity. The most probable scenario is that the buffer is saturated, and then a maximum nominal temperature of 90°C across the whole canister can be assumed. About 20 years after the buffer installation, the temperature of the buffer will reach its peak, and after that, a slight decrease will happen until the buffer and host rock reach the same temperature (Juvankoski, 2013).

The **radionuclide loads** will occur in the case of an accident with the canister. Radionuclides might be released, and thus, protecting the outer environment from these radionuclides is the main objective for the buffer in this scenario. However, all transportation, installation, and application of the buffers are planned in a way to prevent accidents from happening (Juvankoski, 2013).

In conclusion, the mechanical, chemical, thermal, and radionuclide loads shape the behaviour and performance of bentonite barriers. While each load presents distinct challenges, our focus in this study leans towards understanding and mitigating mechanical loads. By comprehensively evaluating these loads, a detailed exploration of the design parameters influencing bentonite's behaviour is conducted in the subsequent chapter. Chapter 2.1.3 analyses the specific design parameters guiding the performance of bentonite barriers, aiming to meet the strict performance targets and design requirements essential for the success of the final disposal concept.

2.1.3 Bentonite Barrier Design Parameters

The previously explained loads must be considered when choosing the buffer design parameters. The first design parameter to consider is what bentonite type to use for the final disposal concept. The first design requirement demands that it must be a natural swelling clay. Accordingly, the reference material used in the buffers for the final disposal concept is Wyoming Sodium Bentonite, previously with the tradename MX-80. The reference material is mined in Wyoming, USA, with a required montmorillonite content of 75-90%. However, if another bentonite type were found with similar properties that fulfil the same requirements, that bentonite type would also be eligible for use in the final disposal concept (Juvankoski et al., 2013).

The second design parameter to be considered is the dimensions of the bentonite barrier. The dimensions of the outer ring, inner ring, and center blocks were presented in **Figure 2**, which included an overview of the three possible bedrock hole sizes. The diameter of the deposition holes for all three versions is 1750mm. This means that the diameter for the block assemblies will be 1650mm, thus leaving a 50mm gap between the outer edge of the buffer and the bedrock. The inner diameter on the canister level is 1120mm, leaving a 35mm gap between the inner diameter for the bentonite buffer and the canister. Both these gaps will be filled with pillow-shaped bentonite pellets to fill the empty spaces. The deposition hole heights vary between the three versions, where LO1-2 has a height of 6640mm, OLI1-2 7870mm, and OL3 8310. The height of the bentonite blocks depends on where the blocks are placed. The blocks are placed underneath the canister, lined with the canister, and above the canister, and their respective block height can be found in **Figure 2**. With these heights, the bentonite block assemblies will be eight layers of blocks above the canister, two layers of blocks underneath the canister, and either 11, 15, or 16 layers of blocks around the canister for LO1-2, OL1-2, and OL3, respectively (Muuri, 2021).

Choosing the correct density for the bentonite buffer blocks is critical to fulfilling several performance targets and design requirements. The density will directly correlate with how well the swelling capacity of the bentonite barriers. Furthermore, the density will also determine how well the bentonite barrier conducts water. At high buffer densities, the transport of chemical species is limited to diffusion and the microbes are not expected to stay active (Posiva Oy, 2016b). Thus, the high enough density ensures the fulfilment of several performance targets and design requirements. However, in bedrock shear displacement scenario, low enough density is needed for mechanical protection of the canister, since the mechanical properties are strongly correlated to the density (Pulkkanen, 2019). The design requirement for sudden rock shear movements limits the upper boundary for the saturated buffer density at 2050 kg/m^3, and the design requirement for limiting the microbial activity determines the lower boundary level at 1900 kg/m^3 (Juvankoski, 2013). Therefore, the blocks should be compacted to have a nominal design bulk density of 1973 kg/m^3 (Muuri, 2021).

The aimed initial water content for the bentonite barriers is 17% (Muuri, 2021). However, after installation, groundwater will gradually saturate the barriers meanwhile the bentonite close to the canister may dry due to the heat produced by the spent fuel. Eventually, the decay heat power decreases and full saturation is achieved. The process of reaching the final saturation might take thousands of years. It might not happen homogenously, which makes both the low and high water contents interesting for experimentation and analysis (Pulkkanen, 2019). The salinity of the groundwater also affects the swelling pressure of the bentonite barriers. As most deposition holes are drilled at 400 meters, the salinity of the water is usually below ten g/L. At this level, a brackish chloride water low on sulphates is most common to encounter bentonite barriers (Muuri, 2021).

One of the design requirements listed is to limit the microbial activity. To limit microbial activity, several different actions should be taken. The first way to limit microbial activity is to control the sulphur-, sulphide-, and organic carbon levels. These levels cannot exceed 1 wt.-%, 0.5 wt.-%, and 1 wt.-% respectively (Muuri, 2021). The second way to limit microbial activity is to have a sufficiently fine pore structure. The pore structure is dictated by the dry density, and a minimum dry density of 1050 kg/m^3 is needed to fulfil the requirement for pore structure. A high enough saturated bentonite buffer also suppresses microbial activity (Muuri, 2021). The rest of the design requirements can be fulfilled mainly by choosing the correct density for the bentonite buffer. The hydraulic conductivity cannot exceed 10^{-12} m/s, achieved by having a dry density of at least 1200 kg/m^3. The density limits will vary from case to case, and a corresponding density will be decided from batch to batch (Muuri, 2021).

To conclude, the design parameters outlined for bentonite barriers are essential for ensuring the success of the final disposal concept. Factors such as selecting the appropriate bentonite type, determining dimensions, and controlling density and water content are critical in meeting performance targets and design requirements. While fulfilling these parameters is crucial, there exists an opportunity for exploration and experimentation to identify alternative configurations that could enhance the effectiveness of the barriers.

2.1.4 Bentonite Barrier Production Process

The production process of the bentonite buffer for the final disposal concept is well documented and consists of several steps, including multiple inspection stages. The production process consists of five main steps: material procurement, manufacturing, storage and transportation of components, preparation of deposition drift, and emplacement of the bentonite buffer. The current production process is designed and valid for the Wyoming sodium-type bentonite (Posiva Oy, 2016a).

The bentonite grains are shipped to the destination in flexible intermediate bulk containers. During transportation, bentonite cannot be in contact with any water, vapour, or other liquids. Therefore, the containers need to be water vapour resistant. At arrival, the bentonite is inspected and stored in an intermediate storage. Before compaction, the bentonite might undergo preliminary steps such as drying and grinding. After that, the bentonite is wetted to a suitable water content and then stored in a silo to achieve moisture equilibrium in its wait to be compacted (Posiva Oy, 2016a).

The optimal production compaction method for the bentonite buffers is still under investigation, and the most suitable method is still to be determined. However, according to (Posiva Oy, 2016a), the reference method for manufacturing bentonite blocks is isostatic compaction. During the isostatic compaction, the final bulk density is determined. During this process, the material is encapsulated in a flexible, impenetrable mould and placed in a pressure vessel. Hydrostatic pressure up to a desired level will then compress the mould homogenously. The mould works both as the forming entity and as the protective barrier against the pressurized liquid (Posiva Oy, 2016a). The following chapters will examine the theoretical framework behind compaction further. After the blocks are compacted, they are checked for cracks and failures. Then, the compacted blocks are machined to fit the dimension requirements presented in Chapter 2.1.3.

The bentonite blocks have achieved their final desired dimensions and bulk density and are thus ready to be shipped to the repository site. During transportation from the manufacturing plant to the repository site, the bentonite blocks are protected from moisture and temperature by being placed in specially designed airtight cases. Upon arrival, they are placed in intermediate storage before being transported to the bedrock level by lift, where they are ready for installation (Posiva Oy, 2016a). This detailed production process ensures that the bentonite buffers meet all design requirements and performance targets, which are crucial for the safe containment of nuclear waste.

2.2 Compaction

Compaction is commonly defined as an irreversible modification in porosity due to the alteration of the granular structure, leading to a permanent decrease in volume. Compaction is a form of compression where the air is removed from the void spaces within the soil. During compaction, the density of the particulate material increases (Sawicki & Swidzinski, 1995).

When performing a compaction test of soils or powders, several different laboratory tests can be conducted. The two most common ones are the oedometer test and isotropic volumetric compaction, which is often referred to as isostatic pressing. The oedometer tests are designed to compress the medium in one dimension by placing the medium in a rigidly confined space that prevents lateral displacement (Yin et al., 2020b). In isotropic compaction, the material is compressed with surrounding fluid pressure with a flexible bag or membrane keeping the fluid from entering the material. This thesis will focus on isotropic volumetric compression tests which are more relevant to the experimental setups discussed in the subsequent chapters.

2.2.1 Compaction of Bentonite

The compaction behaviour of soils is characterized by a strong nonlinearity in the stress-strain relationship (Yin et al., 2020b). This nonlinearity also applies to bentonite due to its complex structure. As discussed in Chapter 2.1.1, bentonite is assembled from the 2:1 layer structure on nanometre scale, and the micro- to millimetre scale structure is unorganized, resulting in a porous medium with voids between the particles. The swelling of this complex structure when saturated with water is a key characteristic of the bentonite used in the final disposal concept. Three different compression mechanisms affect the granular structure during the compaction of such porous mediums. One or more of these mechanisms can occur simultaneously within the granular structure (Davison, 2001):

1. **Rearrangement of grains**: The grains maintain their original size but become more densely packed.
2. **Fracture and rearrangement of grains**: The grains break into smaller grains as they become more densely packed.
3. **Distortion or bending of grains**: The grains undergo deformation due to distortion and bending.

Soils are regularly under cyclic loadings due to natural occurrences such as earthquakes, waves, and winds. Therefore, it is crucial to examine soils and bentonite's mechanical responses in cyclic loading conditions. However, the reason why cyclic pressure programs are used in this thesis is to be able to distinguish between elastic and plastic deformations based on the experimental data. In **Figure 8**, the blue line represents the unloading phase of the compaction, and the pink line represents the reloading of the compaction. The isotropic compaction cycles of bentonite usually involve increasing stress for each cycle. This cyclic compaction helps differentiate between elastic and plastic deformations. During unloading, the grains do not return to their original position, leading to plastic deformation. Because of this, the first loading cycle deforms more volume than the subsequent cycles. Initially, the bentonite is loosely packed, allowing for more plastic deformation, whereas in the latter cycles, the bentonite is denser and less likely to deform plastically.

2.3 Elastoplastic Volumetric Compression Models

Elastoplasticity is defined as "the state of stress between the elastic limit of a material and its breaking strength in which the material exhibits both elastic and plastic properties" (Merriam-Webster, 2024). This chapter provides the theoretical foundation for elastoplastic models. Before presenting the models, key concepts are explored, such as elasticity and plasticity, strain and stress, isotropic elasticity, yielding and yield surface, and the impact of water content on bentonite. Understanding these concepts is essential for developing accurate and reliable mechanical models for bentonite.

2.3.1 Elasticity and Plasticity

Elastic responses are a straightforward process to comprehend, as they involve a recoverable deformation. When a load is applied to a body and then released, the material returns to its original shape, resulting in an elastic deformation (Wood, 1990). Conversely, when a load is applied and then released, but the material does not return to its original shape, plastic deformation occurs (Lubliner, 2008). Typically, the deformation of a body consists of both elastic and plastic deformations.

Most of the research about soil mechanics focuses on predicting plastic deformations and the role of elasticity in soil mechanics might be a bit left out. For regular isotropic linear elastic materials, it can be proven that Young's modulus E and Poisson's ratio v are enough to describe a material's elastic response. Young's modulus is expressed as (Wood, 1990):

$$E = \frac{P/A}{\delta l/l}, \tag{2.1}$$

where P is the load, A is the area, l is the length, and δl is the extension or contraction of the body. Poisson's ratio is expressed as:

$$v = \frac{-\delta d/d}{\delta l/l}, \tag{2.2}$$

where d is the original diameter and δd is the change in diameter. However, in some instances when examining the elasticity of soils, it is beneficial to use two other constants, the bulk modulus K and the shear modulus G, which can be used alternatively to describe the isotropic linear elasticity. They can be expressed with Young's modulus and Poisson's ratio as (Yin et al., 2020b):

$$K = \frac{E}{3(1-2v)}, \tag{2.3}$$

and the shear modulus G can be expressed as:

$$G = \frac{E}{2(1+v)}. \tag{2.4}$$

By using bulk modulus and shear modulus, a more accurate elastic deformation can be described because soils undergo both compressive and shear stresses which are better described with these two constants (Wood, 1990).

As described in Chapter 2.2.2, bentonite consists of grains of various sizes. Thus, most of the plastic deformation of bentonite results from one of the three-grain mechanisms previously described. During these mechanisms, the bentonite undergoes drastic volume changes, making traditional small deformations theories developed for metals less accurate when examining soils like bentonite (Lubliner, 2008).

2.3.2 Stress and Strain

Instead of measuring stress when examining soils, the typical measurable quantity is force. Two types of forces can act on a body: volume mass forces and surface tractions. Stress is the reaction of these forces. In most cases, gravity is the primary volume mass force, while the dominant forces considered in this thesis are surface tractions. The reaction to surface forces is described with the stress tensor (Lubliner, 2008; Puzrin, 2012; Yin et al., 2020b):

$$\sigma_{ij} = \begin{bmatrix} \sigma_{11} & \sigma_{12} & \sigma_{13} \\ \sigma_{21} & \sigma_{22} & \sigma_{23} \\ \sigma_{31} & \sigma_{32} & \sigma_{33} \end{bmatrix} \tag{2.5}$$

The stress tensor is symmetric and σ_{11}, σ_{22}, and σ_{33} are referred to as the normal stresses acting perpendicular to the body. The remaining components are shear stresses acting parallel to the body, denoted in the Cartesian coordinates, such as τ_{xy} for σ_{12} (Lubliner, 2008). The stress tensor can be split to hydrostatic pressure and deviatoric stress parts as:

$$\sigma = -p\mathbf{I} + \mathrm{dev}(\sigma), \tag{2.6}$$

where the hydrostatic pressure is:

$$p = -\frac{1}{3}\mathrm{tr}(\sigma), \tag{2.7}$$

and the deviatoric part is:

$$\mathrm{dev}(\sigma) = \sigma + p\mathbf{I}. \tag{2.8}$$

Similarly to stress, two different strains can be identified: (1) the normal strain and (2) the shear strain. Normal strain refers to the elongation or contraction of a segment, while shear strain is the change of angle between two segments that were initially perpendicular. Strain is a ratio of two lengths and, therefore, a dimensionless unit. The strain tensor defines the strain under small deformations (Puzrin, 2012; Yin et al., 2020b):

$$\varepsilon_{ij} = \begin{bmatrix} \varepsilon_x & \frac{1}{2}\gamma_{xy} & \frac{1}{2}\gamma_{xz} \\ \frac{1}{2}\gamma_{yx} & \varepsilon_y & \frac{1}{2}\gamma_{yz} \\ \frac{1}{2}\gamma_{zx} & \frac{1}{2}\gamma_{zy} & \varepsilon_z \end{bmatrix}, \tag{2.9}$$

where γ is the engineering shear strain. Similarly to the stress tensor, the strain tensor can be split into volumetric and deviatoric parts as:

$$\varepsilon = \mathrm{tr}(\varepsilon)\mathbf{I} + \mathrm{dev}(\varepsilon), \tag{2.10}$$

where the volumetric strain is:

$$\varepsilon_v = \mathrm{tr}(\varepsilon), \tag{2.11}$$

and the deviatoric strain is:

$$\mathrm{dev}(\varepsilon) = \varepsilon - \varepsilon_v\mathbf{I}. \tag{2.12}$$

In this thesis, the focus is on characterising bentonite's volumetric isotropic compression behaviour experimentally and developing volumetric constitutive models. In other words, the aim is to find the relation between the volumetric strain and hydrostatic pressure. The experiments and constitutive relations for shear behaviour is left for subsequent work.

2.3.3 Large Deformation Volumetric Strain

As equation 2.11 mentions, the volumetric strain for linear small deformations can be calculated as the trace of the strain tensor. However, when dealing with bentonite under compaction, the deformations can be significant and this approach for strain is no longer sufficient. To accurately account for large deformations bentonite undergoes during compaction, the approach by Pulkkanen (2019 and subsequent work) is followed.

For large volumetric deformations, the Jacobian of the deformation gradient is introduced. The Jacobian is a measure of the volume change produced by deformation and can be expressed as (Pulkkanen, 2019):

$$\mathrm{J} = \det(\mathrm{F}) = \frac{dV}{dV_0}, \tag{2.13}$$

where F is the deformation gradient. The Jacobian is important when the material undergoes significant volumetric changes as this allows for measurement of how much soil or clay compacts under load. Additionally, when dealing with large deformations, a more realistic way of calculating strain is to calculate the logarithmic strain, also called true strain or Hencky strain. The logarithmic strain introduces the natural logarithm to the strain calculations, and the true volumetric strain can therefore be expressed as (Hencky, 1928):

$$\varepsilon_{v,true} = \ln\left(\mathrm{tr}(\varepsilon_{ij})\right) \tag{2.14}$$

However, to take into account accurate measurement for large deformations, equation 2.13, the volumetric strain becomes:

$$\varepsilon_v = \ln(\mathrm{J}). \tag{2.15}$$

After that, porosity needs to be taken into consideration. This model considers the solid materials, the bentonite grains and water, to be incompressible. This leads to the pore space being the only thing able to be compacted. Therefore, the relative change in pore space is measured before and after compaction, and the decrease in pore space serves as the volume change. It can also be assumed that the smaller the porosity, the more difficult it is to compress the material. Therefore, the strain considers porosity in the following way:

$$\varepsilon_{vol} = \ln(\mathrm{J}_\Phi), \tag{2.16}$$

where J_Φ is the Jacobian that accounts for porosity.

2.3.4 Isotropic Volumetric Compaction

In an isotropic volumetric compaction, all the stresses are equal in all directions, as illustrated in **Figure 7**.

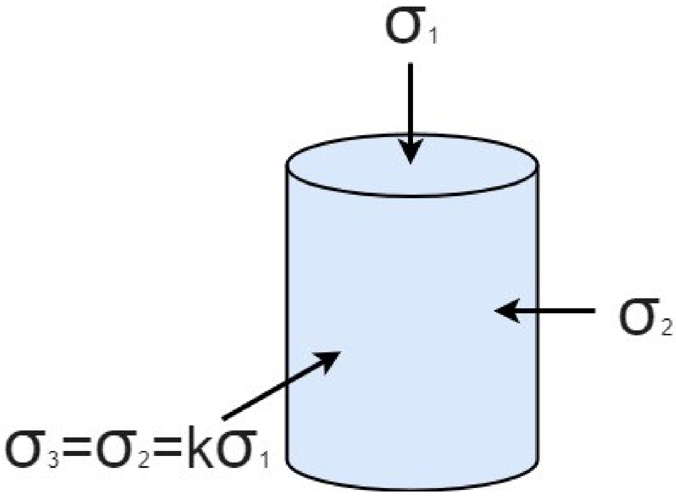

Figure 7: Triaxial compression test stresses (Yin et al., 2020a).

The mean stress acting on the sample can be calculated as:

$$p' = \frac{\sigma_1 + \sigma_2 + \sigma_3}{3}. \quad (2.17)$$

The volume after compaction is given by:

$$V = V_0 - \Delta V_w, \quad (2.18)$$

where V_0 is the original volume and ΔV_w is the volume reduction due to compaction. The volumetric strain is calculated as:

$$\varepsilon_V = \frac{\Delta V}{V_0}. \quad (2.19)$$

A volumetric strain occurs when the mean stress is either increased or decreased, and the volume of the medium will change accordingly (Davison, 2001; Yin et al., 2020a). As the isotropic stress is applied and increased, the sample experiences a uniform compaction in all directions, resulting in a reduction of volume and an increase in strain. In this thesis, the material under compaction is considered isotropic, and therefore, anisotropic material's behaviour is considered out of scope for this thesis. This relationship between stress, strain, and volume change is critical for understanding the mechanical behaviour of bentonite during compaction. **Figure 8** illustrates the relationship between increased stress, resulting strain, and volume decrease during isotropic compaction.

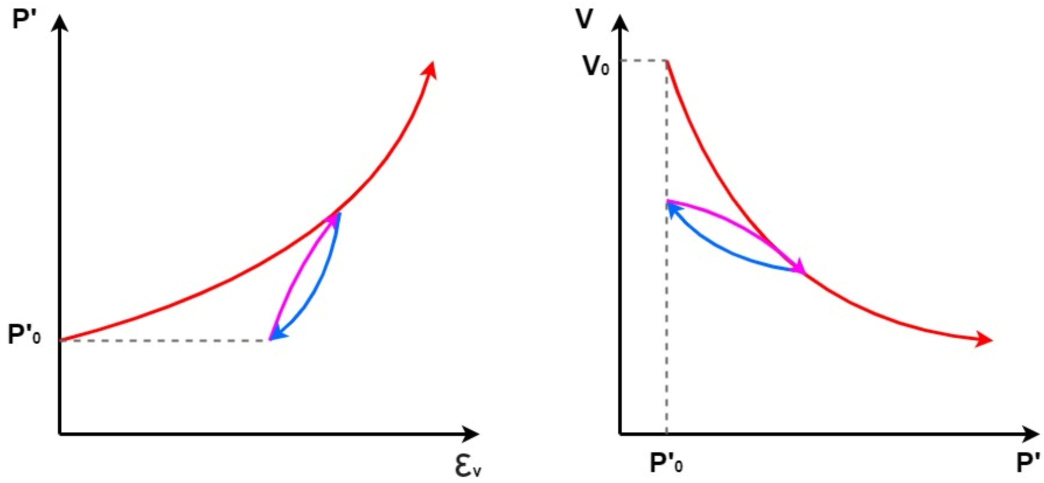

Figure 8: Typical loading behaviour for soils with loading and unloading phases illustrated. (Davison, 2001).

It is essential to understand the relationship between stress, strain, and volume change under isotropic compaction to accurately model the mechanical behaviour of bentonite. Performing isotropic compactions under controlled stress environments allows for the precise calculation of volumetric strain and stress, providing a foundational understanding of the subsequent analysis of bentonite compaction.

2.3.5 Linear Isotropic Elasticity for Volume Changes

When dealing with isotropic materials that are subjected to hydrostatic pressure, as this thesis does, the relationship between pressure and volume change can be treated as a linear relationship for small deformations. This relationship can be expressed with the *coefficient of hydrostatic compression*, also referred to as the bulk modulus K, as (Landau et al., 2012):

$$p = -K\varepsilon_V \tag{2.20}$$

According to it, the bulk modulus K linearly relates to the pressure to the volume change in the material. However, as mentioned in Chapter 2.2.1, bentonite is characterized by a strong non-linearity in its pressure and volume relationship. Bentonite's fundamental properties and variations in density are where this non-linear relationship arises. Therefore, for the scope of this thesis, shear stresses are not taken into consideration, and instead, the primary focus is on understanding how hydrostatic pressure affects volume changes.

2.3.6 Yielding and Yield Surface

Initially, when a material like bentonite, is subjected to hydrostatic pressure, it undergoes purely elastic deformations. If the hydrostatic pressure continues to increase, it will eventually reach a new threshold of the highest pressure the material has withstood. This threshold is referred to as the *yield point* (Wood, 1990). The material will start to deform plastically after the applied pressure has met the yield point, which means that in the relevance of this thesis, some of the volume reduction bentonite undergoes becomes permanent. The yield point for soils can also be referred to as the *consolidation point*. The consolidation point determines where the material transitions from strictly elastic behaviour to elastoplastic behaviour. If the consolidation point increases when it is met, the behaviour is called hardening plasticity. In such case, the more the consolidation point increases, the harder it is to reduce the material's volume permanently.

This thesis focuses on volume changes due to hydrostatic pressure changes, but the basic information of general plastic behaviour is also discussed. If plastic deformation due to shear stress is considered in addition to the hydrostatic pressure, the yield limit is often expressed as a yield surface in principal stress space. The *yield surface* is a surface or hypersurface that represents the boundary between elastic and plastic volumetric behaviour. The stress point inside the yield surface indicates that the material behaves elastically, whilst a stress point extending the boundary of the yield surface indicates that the material enters the plastic stage, where volume changes become permanent. When the boundary of the yield surface is reached and pushed further, it remains expanded. An expansion in the yield surface indicates that the material becomes more resistant to further plastic deformation, a phenomenon called *strain-hardening*. For materials that exhibit hardening, such as bentonite, a higher pressure is required to cause additional plastic deformations (Lubliner, 2008; Puzrin, 2012). If the yield surface contracts, the behaviour is called strain-softening.

For soil materials, the yield surface is often ellipsoid-like around the hydrostatic axis and the consolidation point determines the ellipsoid end on the hydrostatic pressure axis. In Cam-Clay (Yin et al., 2020b) and derivative models, the hardening and softening behaviour is described mathematically with the evolution of the consolidation point.

2.3.7 Water Content of Bentonite Clay

The water content of bentonite significantly impacts its mechanical behaviour. The simplest way to calculate bentonite's water content is the ratio between the water mass and the dry mass of the soil particles (Dueck & Nilsson, 2010):

$$w = \frac{m_{water}}{m_{dry\ mass}} = \frac{m_{total} - m_{dry\ mass}}{m_{dry\ mass}}. \quad (2.21)$$

To fully understand how water affects bentonite, it is essential to understand its structure when water is involved. The bentonite can be divided into sections to clarify its composition further, as illustrated in **Figure 9**.

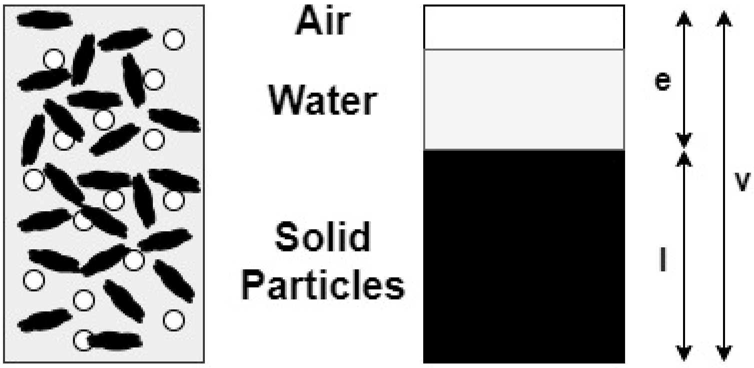

Figure 9: Bentonite's composition is shown as a mixture of the different elements and bentonite's composition with clear divisions between the components (Wood, 1990).

Once the structure is understood, the *void ratio* can be calculated. The void ratio is the ratio between the volumes of voids (water and air) and the volume of soil particles. If the water content and the specific gravity of the material (G_s) are known, and full saturation is obtained, the void ratio (e) can be calculated as (Wood, 1990):

$$e = G_s w. \quad (2.22)$$

The void ratio is a fundamental variable when analysing soils. The above equation can only be applied when soils or clays are saturated, as unsaturated soil conditions introduce additional complexities such as air voids and varying saturation degrees. To calculate the void ratio for unsaturated soils, further knowledge about the degree of saturation (S_r) is required. When the void ratio is known, it can be used to calculate the total porosity of the soil as follows (Wood, 1990):

$$\Phi_{tot} = \frac{e}{1+e}. \quad (2.23)$$

The total porosity is another way of measuring volumetric quantity, representing the ratio of the volume of void to the total volume of the soil. In this thesis, differing from the total porosity definition, the porosity is defined as the ratio of the air (or gas) volume to the total volume of the soil. The porosity can be calculated as (Rotz, 2021):

$$\Phi = \frac{V_G}{V_T}, \tag{2.24}$$

where V_G is the volume of the gas in a sample, and V_T is the total volume of a sample. Another important parameter when dealing with soils like bentonite is dry density. Dry density is the ratio between dry mass and total volume and can be calculated accordingly:

$$\rho_{dry} = \frac{m_{dry}}{V_{tot}}. \tag{2.25}$$

Dry density is a crucial parameter for comparing bentonite samples, as different dry densities result in varying behaviours of the samples. In this thesis, dry density is the primary parameter determining the compaction of each sample. A target value for the dry density is set, and each sample is compacted as close as possible to this target value.

2.3.8 Traditional Elastoplastic Compression Models for Soils

As previously mentioned, the compressive behaviour of soils and clays can be expressed with a non-linear stress-strain relationship. For clays, the pre-consolidation stress (σ'_{p0}), which is the maximum stress the body has been subjected to, plays a vital role when modelling the compression behaviour of bentonite. The volumetric compression behaviour for both elastic and plastic deformations can be measured via the compression curve accordingly (Yin et al., 2020b):

$$\begin{cases} e = e_i - \kappa \ln(\frac{\sigma'_v}{\sigma'_{vi}}) \; at \; \sigma'_v < \sigma'_{p0} \\ e = e_0 - \lambda \ln(\frac{\sigma'_v}{\sigma'_{p0}}) \; at \; \sigma'_v \geq \sigma'_{p0} \end{cases} \tag{2.26}$$

The first equation with kappa (κ) describes the elastic deformations and the second equation with lambda (λ) parameter describes the plastic deformations. These non-linear smooth gradients are visualized in **Figure 10**.

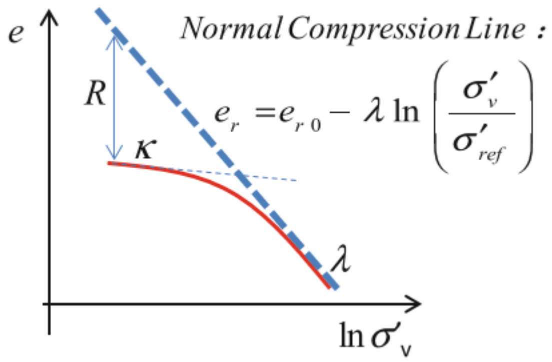

Figure 10: Nonlinear compression characterises for soils and clays, such as bentonite (Yin et al., 2020b).

This approach uses the normal compression line (NCL) as the reference line, which introduces the distance R between the actual state of the soil and the corresponding position on the NCL with an equal value of σ. From this, a nonlinear smooth process that looks the following can be obtained:

$$\Delta e = \kappa \frac{\Delta\sigma'_v}{\sigma'_v} + (\lambda - \kappa)\frac{\Delta\sigma'_v}{\sigma'_v}\frac{1}{1+f(R)}. \tag{2.27}$$

This is one way of modelling the mechanical volumetric behaviour of bentonite using an elastoplastic compression model and the approach is a version of the well-known Cam-Clay model for fully saturated samples and of the Barcelona Basic Model for partially saturated samples. The models are widely used, but allow, for example, negative void ratio in extreme cases but no negative hydrostatic pressure. Fitting the models to experimental data may also require strong idealisation of the observed behaviour. Both Cam-Clay and Barcelona Basic Models also include elastoplastic shear behaviour, which is out of the scope for this thesis.

2.3.9 Large Deformation Elastoplastic Compression Model

The volumetric constitutive model used for fitting to experimental data in this thesis focuses strictly on pure volumetric compaction. The model is built upon the foundational work of Pulkkanen (2019) and subsequent work, which provided the equations and formulas for its development.

The large deformation volumetric strain considering porosity, equation 2.16, is used as the measure for volume change. By implementing the porosity to the formula, the model ensures that the material becomes increasingly harder to compress as the pore spaces in the material decrease, i.e. porosity decreases. It is then possible to model a relationship between the pressure and the volumetric strain with the use of bulk modulus κ for the elastic deformations and with the use of plastic modulus λ for the plastic deformations. The model for the elastic deformations can then be expressed as:

$$p = -\kappa \ln(J_{\Phi e}) = -\kappa \ln\left(\frac{V - V_s}{V_N - V_s}\right), \tag{2.28}$$

where p is pressure, V is the volume during the loading phase, V_s is the asymptotic final volume, and V_N is the initial volume for each loading phase. Similarly, the model for the plastic deformations can be expressed as:

$$p_c = -\lambda \ln(J_{\Phi p}) = -\lambda \ln\left(\frac{V_P - V_s}{V_R - V_s}\right), \tag{2.29}$$

where p_c is consolidation pressure, V_P is the plastic deformation points, V_s is the asymptotic final volume, and V_R is the initial volume for the bentonite sample. Using these models, it is possible to obtain a bulk modulus value, also referred to as kappa values in this thesis, for each sample's elastic deformations and a plastic modulus value, referred to as lambda values, for each sample's plastic deformations. It is, therefore, essential to understand the meaning of these values to draw conclusions.

Elastic Kappa values (κ) represent the compressibility during the initial loading of the bentonite samples, where the material undergoes elastic deformation. The Kappa value is crucial for understanding bentonite's ability to recover its original shape after removing the applied load. The Kappa value can be derived from the slope of the elastic portion of the compaction curve and indicates how much the material compresses within the elastic region.

Plastic Lambda Values (λ) represent the compressibility of the bentonite samples during the plastic deformation phase. During this phase, the material undergoes irreversible changes in the structure. Similarly to the Kappa values, the Lambda values are derived from the slope of the plastic portion of the compaction curve and provide information about bentonite's behaviour under sustained pressure. The Lambda value represents how much the bentonite continues to compress once it has yielded and started to deform plastically.

2.4 Surrogate Models

Surrogate models, also referred to as approximation models (Jiang et al., 2020), are simplified versions of more advanced, high-order models. Surrogate models are typically used within engineering practices to map input data to outputs when the relationship between these factors is unknown.

Surrogate models are particularly effective in scenarios where complicated and time-consuming simulations or experiments exist and the fundamental relationship between the input and output needs to be established (Williams & Cremaschi, 2021).

There are several available surrogate modelling techniques, such as the Polynomial Response Surfaces (PRS) model, kriging models, neural network models, radial basis function models, and more. The most relevant technique for this thesis is the polynomial response surface technique. The PRS methodology determines the relationship between input factors and output responses by utilizing regression analysis and analysis of variance. This approach uses a straightforward polynomial to estimate more complex equations that define the boundary between different states. The general form of the PRS model is (Jiang et al., 2020):

$$f(x) = \beta_0 + \sum_{i=1}^{m} \beta_i x_i + \sum_{i=1}^{m} \sum_{j \geq 1}^{m} \beta_{ij} x_i x_j + \cdots + \varepsilon, \tag{2.30}$$

where ε is the statistical error, x_i is the i-th component of the m-dimensional predicator, and $\beta_0, \beta_{i,}$ & β_{ij} are parameters to be estimated to form column vector $\boldsymbol{\beta}$.

Despite their effectiveness, there are several limitations to response surface surrogate models. One limitation is high-dimensional problems, which means surface surrogate models might become infeasible when the number of explanatory variables is too many. Another limitation is the number of design sites, which means using more design sites increases the computational costs during the fitting process. Additionally, overfitting can occur, where the model captures more random noise in the data than the actual underlying data (Razavi et al., 2012)Despite the limitations, polynomial response surface surrogate models still serve as an effective tool when dealing with uncertain relationships between input factors and output responses, as this thesis does.

2.5 Design of Experiments

To gain more knowledge about the Design of Experiments (DoE), a meeting with Senior Scientist Olli Saarela at VTT was held in April 2024. Saarela provided an in-depth explanation of how DoE works and how to successfully implement DoE:s in a research problem. According to Saarela, a DoE aims to get the maximum amount of information possible with a minimal number of experiments. To create a DoE, the factors (inputs) and the response variables (outputs) need to be defined. Both the inputs and outputs are chosen so they align accordingly to the research objectives. After determining these elements, the optimal design setup should be explored. The two main design principles for DoE:s are full factorial designs and fractional factorial designs (Saarela, 2024), as shown in **Figure 11**.

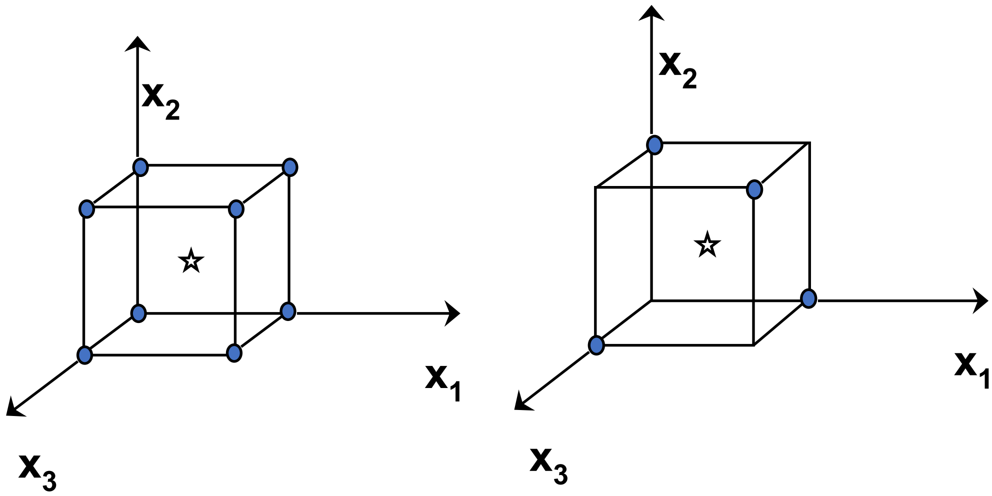

Figure 11: Full factorial design (left) and fractional factorial design (right). X-axes represent the input variables and the blue dots indicate the experiments required. The star represents the centre point experiment (Saarela, 2024).

In a full factorial design, all possible experiment scenarios are conducted, which also gives more reliable results. In a fractional factorial design, the experiments are selected in an optimized manner to test all input variables with a limited number of experiments. A fractional factorial requires an even distribution and good coverage between the input variables to work properly. If the experiments are repeated, it will yield a more reliable analysis (Saarela, 2024). This introduction was used to define the DoE conditions for this thesis, which are presented in Chapter 3.2.

3 Methodology

The following chapters will present the new compaction station and explain the methodology for this thesis.

3.1 New Compaction Station

The new compaction station was planned, built, and tested between February 2023 and January 2024 as part of the authors' duties as a Research Trainee at VTT. The limitations of the old compaction station were briefly described in the introduction in chapter 1.1.2. A summary of the limitations includes:

- Using a single device for both volumetric compaction and shearing leads to a higher usage rate and, thus, limited availability. Additionally, having only one device makes the system vulnerable to breakdowns.
- The old compaction station's maximum achievable pressure is 32MPa, which limits the highest density the bentonite samples can achieve.
- The pressurised fluid used is silicon oil, which is messy, and can create inaccuracies during the compaction phase.

Therefore, the objectives for the new compaction station can be summarized as:

- Create an independent compaction station, separate from the shearing station, to increase availability and reduce vulnerability to breakdowns.
- Ensure the new compaction station can achieve maximum pressure above 32MPa.
- Use a more accurate and less messy pressurised fluid than silicon oil.
- Be able to control the test procedure on a designated desktop computer.
- Be able to run cyclic compaction programs to easily distinguish between elastic and plastic deformations.

With the objectives clearly defined, the following step was to develop an initial design for the new compaction station.

3.1.1 Initial Design for New Compaction Station

The first critical step in planning the new compaction station was to decide which pressurised fluid to use. De-aerated water was quickly chosen for several reasons. De-aerated water is water in which all air is removed, making it suitable for compaction due to its incompressibility. Additionally, de-aerated water is easy to handle and easily available. After selecting the fluid, an initial design for the device was developed, as shown in **Figure 12**.

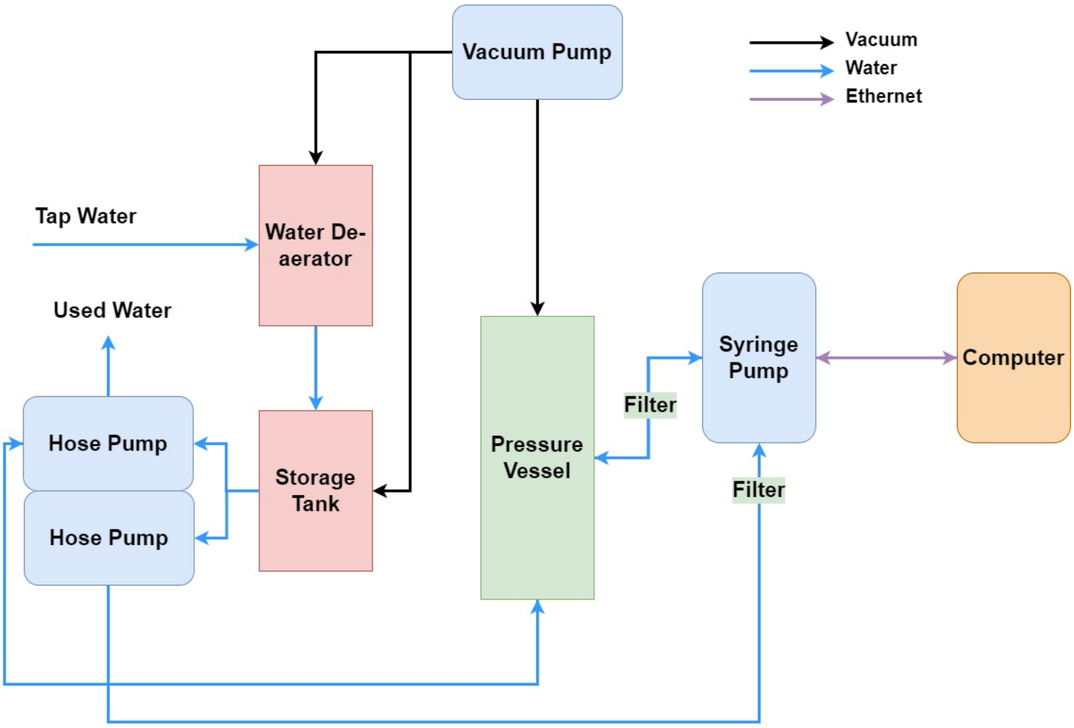

Figure 12: The initial design for the new compaction station.

The suggested design works by loading the de-aerator with regular tap water. The water de-aerator works by having a rapidly rotating impeller that causes cavitation, rapidly removing the dissolved gasses in the water. The de-aerator needs a vacuum to work. After de-aeration, the de-aerated water is transported to a storage tank, where a vacuum is also required to keep the de-aerated water stable. Two separate hose pumps are then connected to the storage tank to distribute the water to the pressure vessel and the syringe pump. A connection between the pressure vessel and the syringe pump is established to regulate pressure. An internet connection is established between the syringe pump and a desktop computer so compactions can be run and monitored remotely. Post-compaction, the used water is pumped away into the sink by the hose pump connected to the pressure vessel. The initial design served as a foundation for designing the new compaction station. The following subchapter discusses the equipment used and the setup for the new compaction stations.

3.1.2 Equipment Used and Setup

After establishing the initial design, all the necessary equipment was ordered or picked up from the inventory and subsequently set up. The following equipment was used:

No	Equipment	Model	Total
1	Syringe Pump	Floxlab BTSP 175-15	1
2	Water De-Aerator	GDS Nold DeAerator	1
3	Storage Tank	GDS Instruments	1
4	Pressure Vessel	Dustec Pressure Vessel 100MPa with quick lock	1
5	Vacuum Pump	Edwards XDS 10	1
6	Hose Pump	Verderflex EV1500	2
7	Electric Chain Hoist	Yale Vego 0,5t	1
8	High Pressure Valves	Parker Autoclave Engineers 1034Bar	4
9	High-Pressure Piping	Parker Autoclave Engineers 1034Bar	3m
10	Low-Pressure Valves	Various Models	9
11	Low-Pressure Piping	Verderflex Tubes	5m
12	Desktop Computer	HP Desktop Computer	1

Table 1: Equipment and total quantity for the new compaction station.

All equipment was then assembled following the initial design. **Figure 13** shows the assembled new compaction station, with numbers corresponding to the equipment listed in **Table 1** for clarity.

Figure 13: The new compaction station setup. The main components are listed with the number according to **Table 1**.

The desktop computer, not visible in **Figure 13**, is connected to the syringe pump by an ethernet cable routed to the ceiling. The highest pressure that is recommended to be applied in the pressure vessel is 1000 Bar (100MPa). The syringe pump and the high-pressure valves recommended max pressure is

1034 bar. The four high-pressure valves are all connected to the pressure vessel to ensure that the system can withstand at least 100 MPa pressure. The following chapter examines the functionality and performance of the new compaction system.

3.1.3 Functionality of the New Compaction Station

The first test compactions for the new station were conducted in the middle of June 2023. Since then, over 100 compactions have been completed successfully, which ensures that the new compaction station operates as expected. Various bentonite configurations have been tested during this time and all different configurations have been successfully completed. To calibrate the new compaction station, a metal dummy was placed inside the pressure vessel, and normal cyclic tests were conducted on the dummy. These calibrations are regularly performed to ensure the accuracy of the station's test result.

The experimental procedure for a sample in the new compaction station can be divided into three main parts: preparation, compaction, and completion. During the preparation stage, the bentonite is mixed into the wanted configuration and then placed in a rubber membrane, according to **Figure 14**. The rubber membrane protects the bentonite from being in contact with the water and also ensures that the effective stress can be fully controlled (Sean, 2013). The preparation stage is then finished.

Figure 14: The first picture shows the metal quick lock. The second picture shows the rubber membrane. The third picture shows the completed setup, where the bentonite is inside the rubber membrane, and the metal lock is attached to it with a hose clamp.

In the second stage, Compaction, the completed setup is attached to the top of the pressure vessel, as shown in **Figure 15**. A vacuum is connected to the sample through the metal quick lock to remove all the air inside the rubber membrane. The pressure vessel is then sealed and filled with de-aerated water. Thereafter, all valves are closed except those between the syringe pump and the pressure vessel. The syringe pump fully controls the effective stress applied to the bentonite sample.

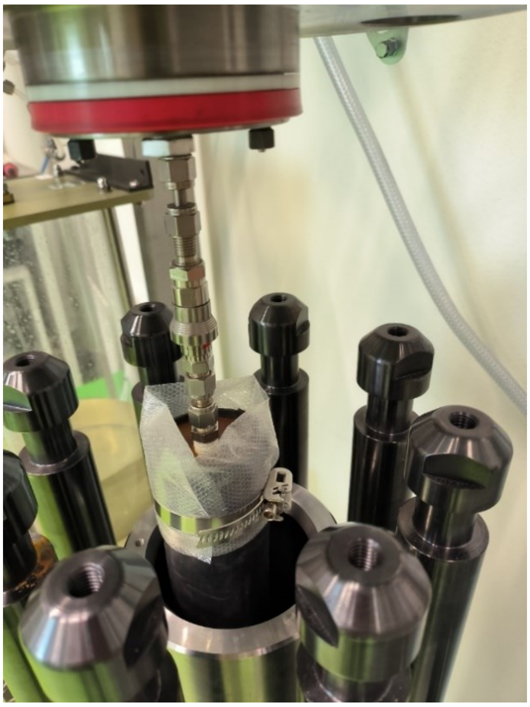

Figure 15: The bentonite setup placed inside the pressure vessel.

At this stage, the compaction program is initiated from the desktop computer. The compaction program consists of several pressure cycles, with the pressure increasing for each cycle. The standard number of pressure cycles used for this thesis is eight cycles, where the four first cycles are 2MPa, 4MPa, 8MPa, and 16MPa. The four remaining cycles are chosen based on the configuration of the bentonite. Between each cycle, the pressure is decreased to 0.75MPa and then increased to the following cycle value. It would be impractical to decrease the pressure all the way to 0MPa due to unstable conditions at such low pressures. The compaction program runs until the pressure returns to 0.75MPa after the last cycle. The data collected during the compaction program is pressure, volume added into the vessel, volume remaining in the high-pressure pump, and the flow rate of the fluid.

The last stage is the completion stage, where the water is removed from the pressure vessel, and the compacted bentonite sample is removed from the rubber membrane. The compacted sample, shown in **Figure 16**, is checked for possible water leaks, then weighed and stored in a vacuum-sealed bag. After the sample is vacuum sealed, the total volume of the sample is measured. This is done by weighing a water bucket’s initial weight, including water, and then adding the vacuum-sealed bentonite sample into it without touching the bottom of the water bucket. The weight increase is registered and based on this increase and water’s density; the total volume of the sample can be calculated.

Figure 16: A compacted bentonite sample.

The functionality of the new compacting station can be confirmed by the large number of samples compacted and regular calibrations conducted thus far. The objectives for the new compaction station, listed in Chapter 3.1, are also fulfilled. The new compaction station uses an easily accessible and reliable fluid as the pressurised fluid, it can reach pressures up to 100MPa, and it is possible to run cyclic pressure programs from a desktop computer. After ensuring the system's functionality, the following is to examine the DoE conditions for this thesis.

3.2 Design of Experiment (DoE) Conditions

Currently, the Nuclear Waste Management research team at VTT has an extensive DoE ongoing, SAGE DoE hereinafter, which includes bentonite type, water content, dry density, shear pressure component, and varying total dissolved solids (TDS) with a constant sodium to calcium ratio as its input variables.

To avoid overlapping with the existing SAGE DoE, discussions with Research Team Leader Veli-Matti Pulkkanen and Research Scientist Anniina Seppälä were held in April 2024. It was decided to exclude factors affecting only the shearing behaviour of the experiments, as this is not the focus of this thesis. Consequently, dry density and shear pressure components were disregarded as possible factors. To keep the number of experiments manageable within the limited timeframe of this thesis, four input variables were selected in the DoE: bentonite type, water content, water salinity, and waiting time.

Bentonite Type

As described earlier, bentonite type is a key factor included in this thesis DoE. The existing SAGE DoE includes three different bentonite types: Wyoming sodium bentonite, Georgian calcium bentonite, and Bulgarian calcium bentonite. The characteristics of the Wyoming bentonite were briefly examined in Chapter 2.1.3. Both Georgian and Bulgarian calcium bentonite are referred to by their origin country and predominant cations.

To keep the number of experiments low but still have a comparison between bentonite types, two bentonite types were chosen for this thesis DoE: Wyoming sodium bentonite and Bulgarian calcium bentonite. These two were chosen due to having different origins as well as predominant cations. Also, Wyoming sodium bentonite serves as the reference bentonite for bentonite barriers in the final disposal concept by Posiva, making the findings of this thesis applicable to real-world scenarios.

Water Content

The desired initial water content and its effects on the bentonite barriers are explained in Chapter 2.1.3. In the SAGE DoE, five different alternatives for the water content were chosen: 11%, 14%, 17%, 20%, and 23%. These five alternatives cover a broad range from slightly saturated to well-saturated conditions.

In this thesis, three different water content alternatives were chosen: 14%, 17%, and 20%. These alternatives provide an additional comparison to the SAGE DoE. Also, 17% is the desired initial water content for disposal, and with these alternatives, both an under-saturated and an over-saturated alternative is tested.

Water Salinity

In the SAGE DoE, the salinity of the water is chosen to have a fixed Na/Ca ratio with varying amounts of total dissolved solids. The ratio was 3,4375:1, almost 3,5 parts sodium to 1 part calcium. As this approach is already being examined, this thesis took a different approach to the water salinity. This thesis examines a fixed amount of total dissolved solids with a varying ratio of Na/Ca.

To decide the fixed amount of dissolved solids, conversations were held with Principal Scientist Pirjo Hellä and Senior Scientist Paula Keto at the beginning of May 2024, and they indicated that near repository levels, the TDS amount varies between 6 g/l to 20 g/l. Historically, the TDS levels have decreased with time, as shown in **Figure 17** (Posiva Oy, 2021b).

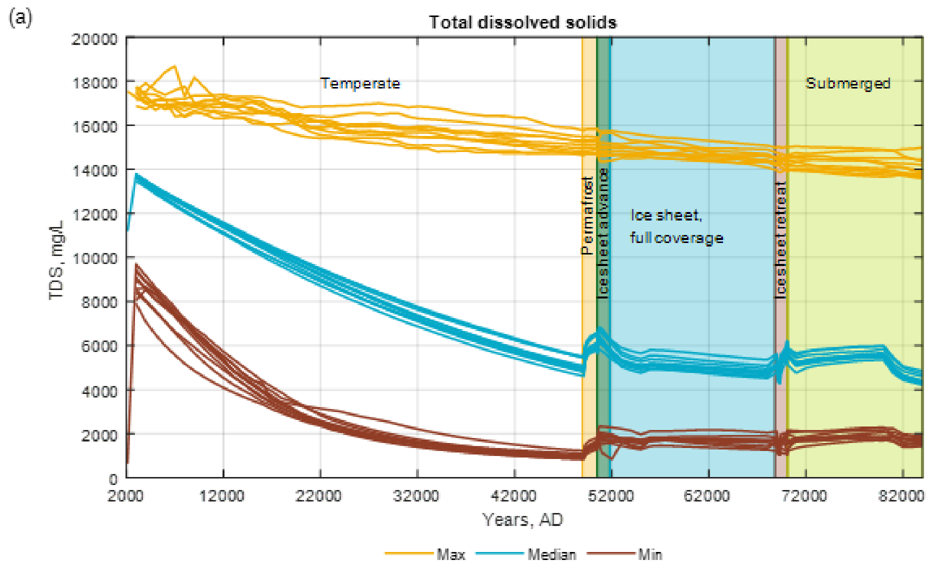

Figure 17: The evolution of total dissolved solids in deposition holes during several time periods (Posiva Oy, 2021b).

Based on the historical decrease in total dissolved solids, this thesis chose a TDS amount of 10 g/l. 10 g/l allows the salinity of the water to exchange cations with the bentonite while remaining a realistic case. In the SAGE DoE, a constant mass ratio between sodium and calcium is examined. Based on onsite data from groundwater samples done by Posiva, the mass ratio between sodium and calcium depends on the TDS, according to **Figure 18**.

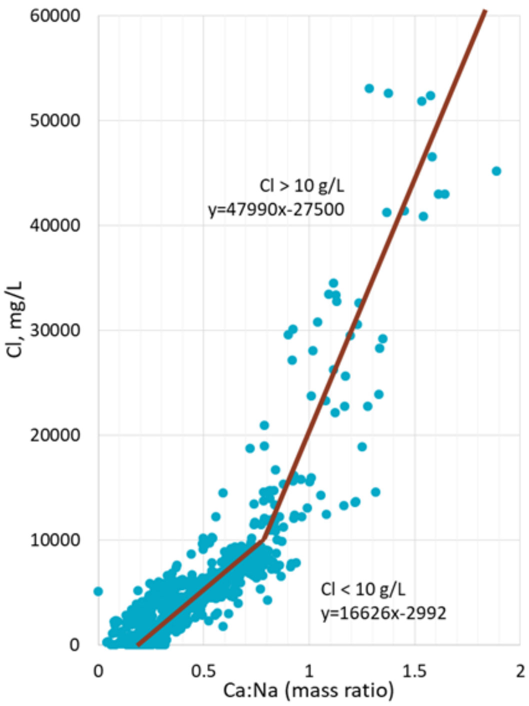

Figure 18: Ca/Na mass ratio compared to the Cl concentration based on groundwater samples. A separate linear function is fitted to concentrations below 10g/l and above 10g/l (Posiva Oy, 2021a).

According to **Figure 18**, the Ca/Na mass ratio is mostly between 0.6 and 0.8 when the TDS is 10 g/l. In this thesis, a mass ratio of 0.667, or two parts calcium and three parts sodium, was chosen as one of the alternatives for the water salinity as this mass ratio represents a realistic case based on groundwater samples. Additionally, two other alternatives were chosen: one alternative with only sodium and one alternative with only calcium. By adding these two alternatives with only one element present, it was possible to distinguish between the effects both elements have on the bentonite buffer.

In summary, three water salinity alternatives were chosen for this thesis' DoE. All alternatives had 10g/l total dissolved solids, and the three mixtures contained only calcium, only sodium, and a 2:3 mass ratio between calcium and sodium.

Waiting Time

During the discussions with Pulkkanen and Seppälä in April 2024, they identified waiting time as a potentially important variable. Waiting time refers to the duration for which partially saturated bentonite is left in a vacuum-sealed bag to react with the salinity of the water. The objective of incorporating waiting time into the DoE is to measure the time-dependent interactions between the saline water and bentonite, which in itself can influence the performance and properties of the bentonite buffer. Waiting time specifically targets the chemical interactions and potential alterations in the bentonite structure over time. Based on this thesis's limited time frame, four different waiting time intervals were selected: 1 day, 5 days, 10 days, and 14 days.

Design of Experiment Creation

The Modde software developed by Sartorius was used to create the DoE table. The D-optimal design approach was chosen for this study. D-optimal designs are computer-generated designs that maximize the determinant of the X'X' matrix, which maximizes the volume of the design space. The D-optimal method minimizes the number of experimental runs while maximizing the information gained. The D-optimal method also ensures the maximal spread of the experiment, which leads to more informative experiments. The following table represents the DoE used in this thesis generated by the Modde software.

Exp No	Exp Name	Bentonite Type	Water Content	Fixed TDS - Na/Ca Ratio	Waiting Time
1	N1	Ca	14	NaCl	1
7	N7	Ca	20	2:3	1
6	N6	Na	14	2:3	1
3	N3	Ca	14	CaCl	1
4	N4	Ca	20	CaCl	1
2	N2	Na	20	NaCl	1
5	N5	Na	17	CaCl	1
9	N9	Ca	17	NaCl	5
8	N8	Na	14	NaCl	5
17	N17	Na	14	CaCl	10
19	N19	Na	20	2:3	10
18	N18	Ca	14	2:3	10
20	N20	Ca	17	2:3	10
10	N10	Ca	14	NaCl	14
11	N11	Ca	20	NaCl	14
14	N14	Ca	17	CaCl	14
16	N16	Ca	20	2:3	14
12	N12	Na	17	NaCl	14
13	N13	Na	20	CaCl	14
15	N15	Na	14	2:3	14

Table 2: The DoE used for this thesis. The table lists each experiment with its respective conditions for bentonite type, water content, Ca: Na ratio, and waiting time. Twenty experiments were generated in total.

Table 2 outlines the specific conditions under which each experimental run was conducted, ensuring that all combinations of the factors are adequately explored to generate comprehensive and reliable data. After the waiting time had reached the specified days, all samples were compacted similarly, as explained in Chapter 3.1.3. The desired dry density for the samples was, with discussion with Pulkkanen, decided to be 1650 kg/m^3. As explained in the Literature Review, a dry density of 1650 kg/m^3 fulfills several of the performance targets and the design requirements. To ensure successful compaction of all samples to the target dry density, a data bank developed by Seppälä containing information on previous compactions was used. The data bank provided information on the specific compaction cycle programs needed to compact a bentonite configuration to the target dry density.

3.3 Calibration of the Compaction Device

To obtain sample volume change by reducing the equipment volume change from the measured total volume change, and to maintain the accuracy and reliability of the experimental results, the new compaction station needs to be calibrated regularly. Calibration of the compaction station ensures that the device operates correctly and that measured volumes are precise and reproducible. The new compaction station was calibrated by placing a cylindrical steel dummy in the same rubber membrane as the bentonite powder would be placed in. After that, the same cyclic compaction program, up to 55MPa, was performed. There were two reasons why the steel dummy was used for the calibration:

1. **Consistency and Invariance**: Steel can be assumed incompressible in the used pressure and thus any variations in the compaction readings are due to the compaction station itself, not the material being compacted. This ensures consistency in the calibration data.
2. **Repeatability**: The steel dummy ensures repeated calibrations under identical conditions. The properties of the steel dummy do not change, and thus, the same readings can be used to verify multiple calibrations.

In total, three calibration tests were conducted while the samples were being produced according to the DoE. One calibration was conducted before producing the samples, one in the middle of the process, and the final calibration after all samples were produced. The raw data from the calibrations can be seen in **Figure 19**.

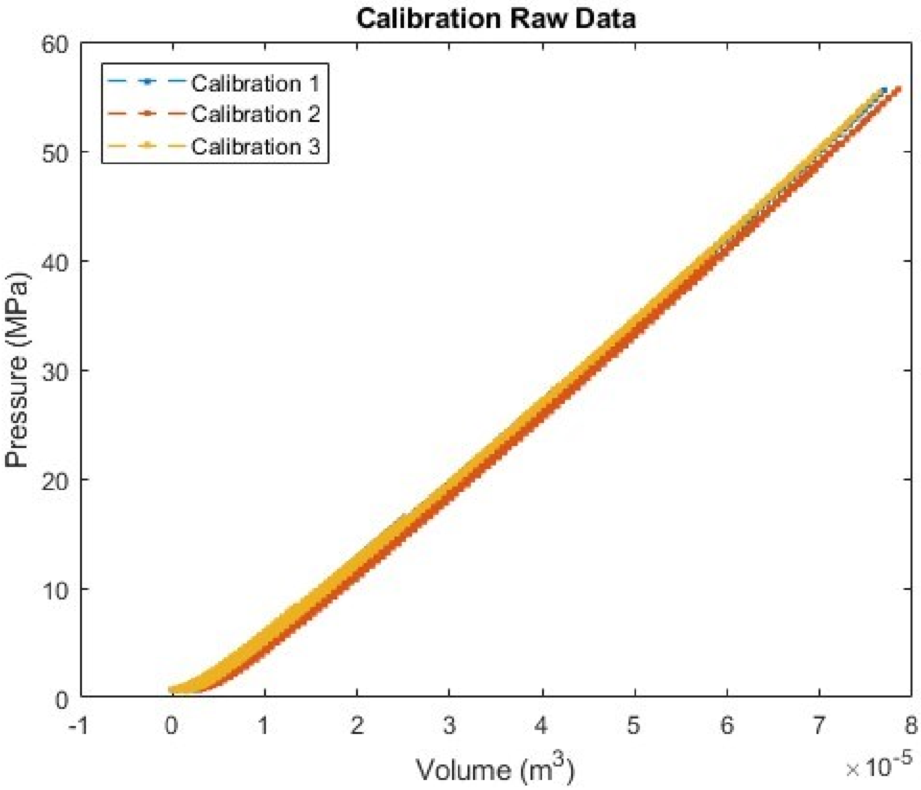

Figure 19: The raw data from the three calibrations conducted while producing samples for the DoE.

By performing three calibrations with the steel dummy, the compaction station's performance is consistently checked and benchmarked against a standard. The results, according to **Figure 19**, are almost identical for calibration one and three while calibration two shows a slight deviation. To measure the difference between the calibrations, calibration one serves as the reference calibration. After that, an interpolation is performed on all three calibration data sets. This interpolation gives all three data sets common volume values and corresponding pressure values. After that, the average percentage difference between the pressure values is calculated with calibration one as the reference calibration. The average Percentage Difference of calibration two relative to calibration one was 4.79%, and for calibration three, 2.12%. Additionally, a comparison of the volume difference at the maximum pressure was conducted. The volume difference at the maximum pressure for calibration two relative to calibration one was 1.70% and for calibration three, 0.29%.

This difference in calibration data might occur from variations in the test setup. For example, several different rubber membranes were used during compactions, and different membranes might have been used during the calibrations. Additionally, there are two different quick locks where the metal cylinder that the quick lock is attached to is of different sizes, one with a diameter of 60mm and the other 65mm. Other factors that might create the differences in the calibration data are instrument calibrations, meaning that the syringe pump also needs regular calibration. There is a difference, however, the difference remains within acceptable limits. Therefore, it can be assured that the calibrations and the test data are accurate. This calibration process is critical for ensuring reliable experimental results.

3.4 Data Analysis

The first step of the data analysis process involved managing the collected data. This included reviewing the compaction data files for missing information and formatting them into the correct condition. The raw data files from the compaction station were in the DAT format and consisted of rows with all necessary information, such as volume and pressure. The next step was to process all the raw data and organize it in a usable manner. This handling was conducted in MATLAB, where each of the 20 experiment files was processed and split into separate cells. Thereafter, a piecewise cubic spline function was fitted to the calibration data and the equipment volume change was subtracted from the experimental raw data. After this step, the data was in the correct format for further analysis.

The following step involves using MATLAB's fit function to obtain both the elastic kappa values (κ) and the plastic lambda values (λ) for each experiment. Kappa and Lambda are fitting parameters that are crucial for understanding the behaviour of compacted bentonite samples under different configurations.

Both (κ) and (λ) were fitted separately to obtain two independent values. The kappa values were obtained by fitting a function to the loading phases. Therefore, the unloading phases are not considered at all, and hysteresis is considered outside of this thesis's scope. The lambda values were obtained by fitting a function to the plastic deformation points. The MATLAB scripts handling the experimental data were written by Pulkkanen, Senior Scientist Sharma Mrityunjai, and the researcher himself. After obtaining both values, the values were put into the Modde software for further analysis. The surrogate models were then developed using Modde software with their built-in features. Two copies of the original DoE in Modde were created, one consisting of the kappa values and one of the lambda values.

4 Results

This chapter presents the results gathered to address the objective of the thesis. Firstly, the necessary auxiliary data is shown, followed by a presentation of the elastic and plastic surrogate models.

4.1 Compaction Data

The compaction of the 20 bentonite samples according to the DoE was successfully finished in the beginning of June 2024. The measurement and calibration data are uploaded to www.bentonitedata.com database. None of the 20 experiments experienced any failures during the compaction program. 18 out of 20 experiments produced a correct data file with all the necessary information, with CC_N14 and CC_N17 having a problem formatting the first two cycles. After compaction, the dry density was measured for each experiment and **Table 3** shows a comparison of the achieved dry densities.

Exp No	Exp Name	Bentonite Type	Water Content	Fixed TDS - Na/Ca Ratio	Waiting Time	Dry Density
1	N1	Ca	14	NaCl	1	1632
7	N7	Ca	20	2:3	1	1615
6	N6	Na	14	2:3	1	1643
3	N3	Ca	14	CaCl	1	1639
4	N4	Ca	20	CaCl	1	1640
2	N2	Na	20	NaCl	1	1665
5	N5	Na	17	CaCl	1	1682
9	N9	Ca	17	NaCl	5	1565
8	N8	Na	14	NaCl	5	1653
17	N17	Na	14	CaCl	10	1585
19	N19	Na	20	2:3	10	1634
18	N18	Ca	14	2:3	10	1501
20	N20	Ca	17	2:3	10	1611
10	N10	Ca	14	NaCl	14	1518
11	N11	Ca	20	NaCl	14	1585
14	N14	Ca	17	CaCl	14	1547
16	N16	Ca	20	2:3	14	1606
12	N12	Na	17	NaCl	14	1689
13	N13	Na	20	CaCl	14	1634
15	N15	Na	14	2:3	14	1654

Table 3: The final dry density for each experiment.

The average dry density for each of the 20 samples is 1615 kg/m3, slightly below the desired 1650 kg/m3. This was expected, as achieving higher dry densities was overall more difficult for the calcium bentonite samples than for the sodium bentonite samples. Also, achieving higher dry densities was more challenging with a higher water content. With a higher water content in the bentonite, the excess water occupies more space between the grains, which reduces the achievable dry density during compaction. Therefore, for samples with calcium bentonite and 20% water content, the highest-pressure cycles in the cyclic compaction program were used. Therefore, the lowest pressure in a cyclic compaction program was used with sodium bentonite and 14% water content. A comparison of CC-N4 and CC-N8 raw data can be seen in **Figure 20**. These two samples have similar dry densities whilst having completely opposite DoE configurations.

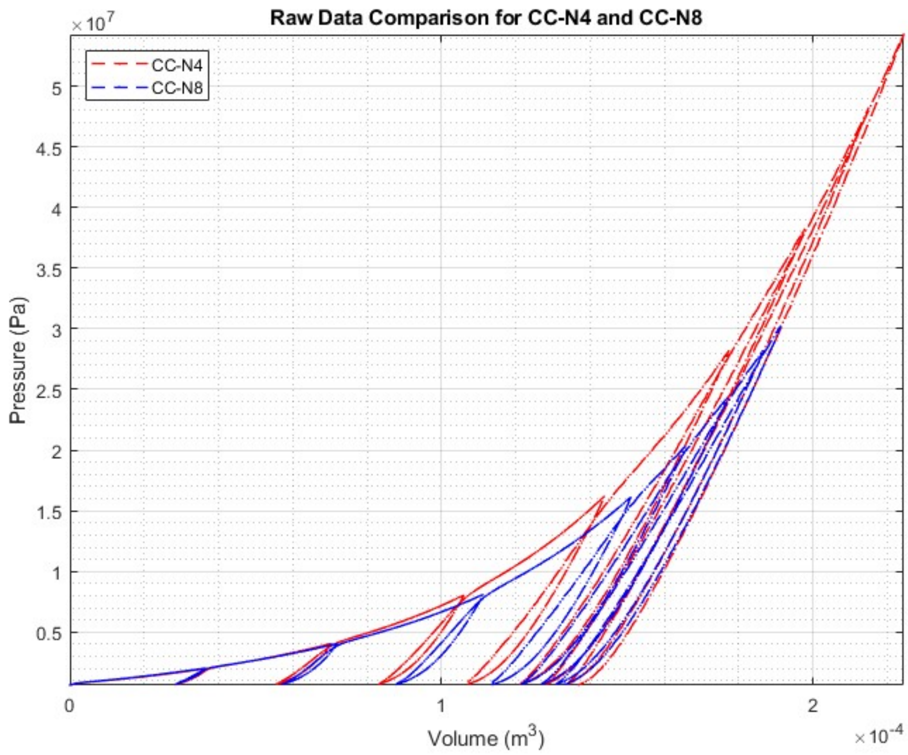

Figure 20: Raw data comparison of CC-N4 and CC-N8 with volume on the x-axis and pressure on the y-axis.

CC-N4 has a dry density of 1640 kg/m3, and the last cycle of the compaction programme is up to 55MPa. CC-N8 has a dry density of 1653 kg/m3, whilst the last cycle only reached 30MPa. This demonstrates that the different configurations require different compaction programs to achieve the desired dry density.

While the raw data is useful to check that all experiments were successfully conducted, it cannot be used for further analysis. The data that should be analysed further is the calibrated data, where any volumetric changes due to the compaction station itself are considered. This is done by fitting a function to the calibration data, seen in **Figure 19**, and subtracting the function from the raw data. This ensures that the compaction data is calibrated and any volumetric changes due to the compaction station are eliminated. The calibrated data for CC-N4 and CC-N8 are shown in **Figures 21** and **22**, respectively.

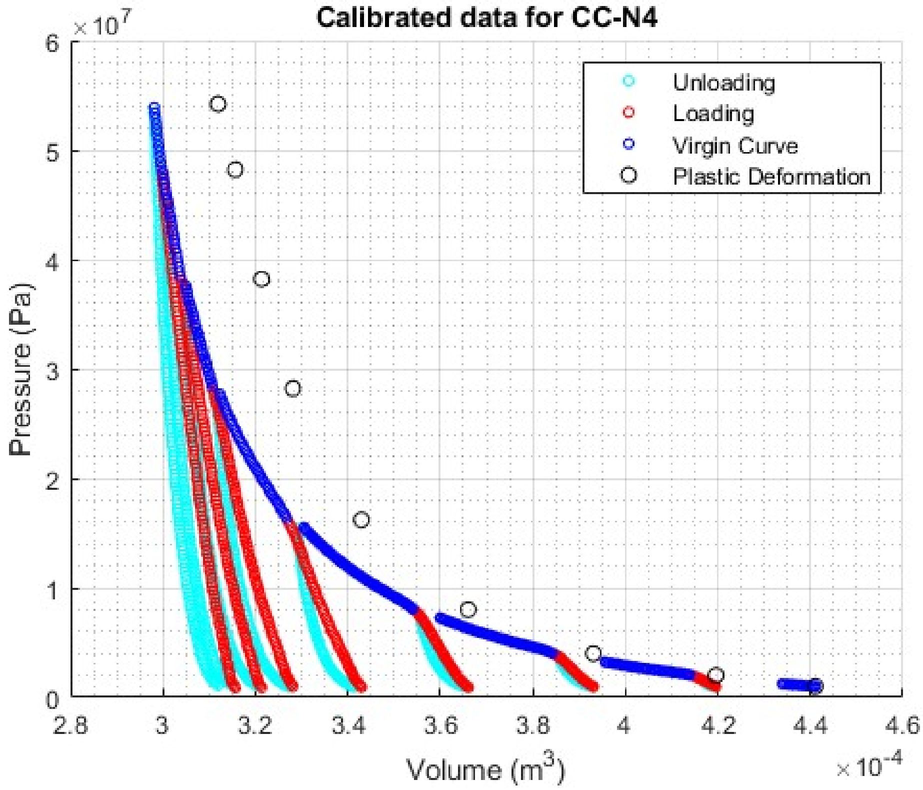

Figure 21: Calibrated data for CC-N4, which shows elastic loading- and unloading phases, virgin curve, and plastic deformation points.

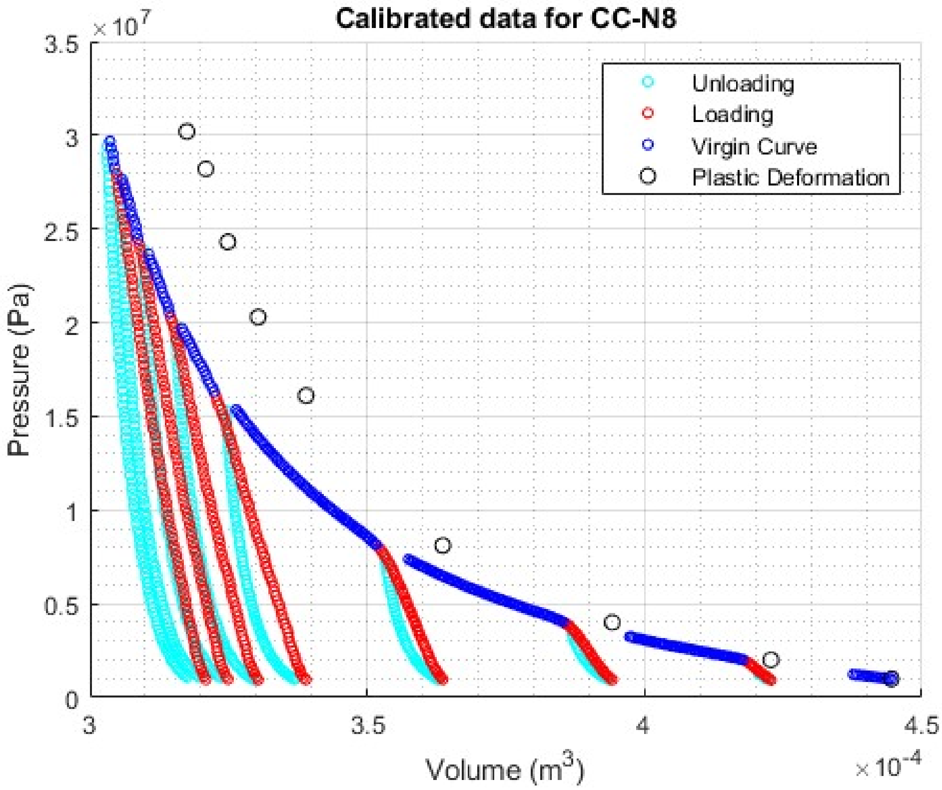

Figure 22: Calibrated data for CC-N8, which shows elastic loading- and unloading phases, virgin curve, and plastic deformation points.

As the figures above show, the data is presented differently compared to the raw data. The raw data shows how much liquid was added to the compaction station, while the calibrated data shows the volume of the bentonite sample. Therefore, the final volume of the bentonite sample can be read from the calibrated data figures as the last point on the last unloading cycle. In contrast, the last point on the raw data cycle indicates how much water was added to the compaction station.

4.2 Lambda and Kappa Values

4.2.1 Kappa Values

The elastic Kappa-values (κ) were obtained by fitting the function mentioned in the literature review, equation 2.28, to the loading phase of the calibrated data. Two approaches were used to calculate two different kappa-values. The first approach to obtain the kappa value for the calibrated data was by calculating an individual kappa for each loading phase. After that, a weighted average was calculated for each kappa based on the number of data points. The second approach calculates a common kappa for each loading phase by using the sum of squared errors. Firstly, a custom model for the relationship between volume and pressure is defined as the function above. Thereafter, an objective function that measures the error between the actual data and the custom model's predicted data is created. The objective function calculates the sum of squared differences between the actual pressure values and those predicted by the custom model. Finally, the fminsearch function is used in MATLAB to obtain the kappa values, which optimizes the kappa value by minimizing the error measured by the objective function. A comparison of the kappa values obtained can be seen in **Table 4**.

Exp Name	Weighted Average Kappa	Common Kappa
N1	3,96E+07	4,38E+07
N2	4,73E+07	3,20E+07
N3	4,92E+07	4,96E+07
N4	5,09E+07	5,57E+07
N5	5,53E+07	4,62E+07
N6	6,80E+07	5,32E+07
N7	5,30E+07	5,63E+07
N8	5,45E+07	4,73E+07
N9	4,04E+07	3,67E+07
N10	5,05E+07	4,72E+07
N11	5,54E+07	6,40E+07
N12	5,40E+07	4,82E+07
N13	4,43E+07	3,55E+07
N14	4,21E+07	4,26E+07
N15	5,99E+07	4,96E+07
N16	5,51E+07	6,27E+07
N17	5,29E+07	4,19E+07
N18	4,80E+07	5,07E+07
N19	5,16E+07	3,36E+07
N20	3,83E+07	4,12E+07

Table 4: Comparison of elastic kappa values obtained by the two approaches.

As shown in the table above, there is a slight difference in the kappa values obtained based on the used approach. A visual comparison of the kappa values is shown in **Figure 23**. The figure lists the DoE conditions for each experimental sample as well.

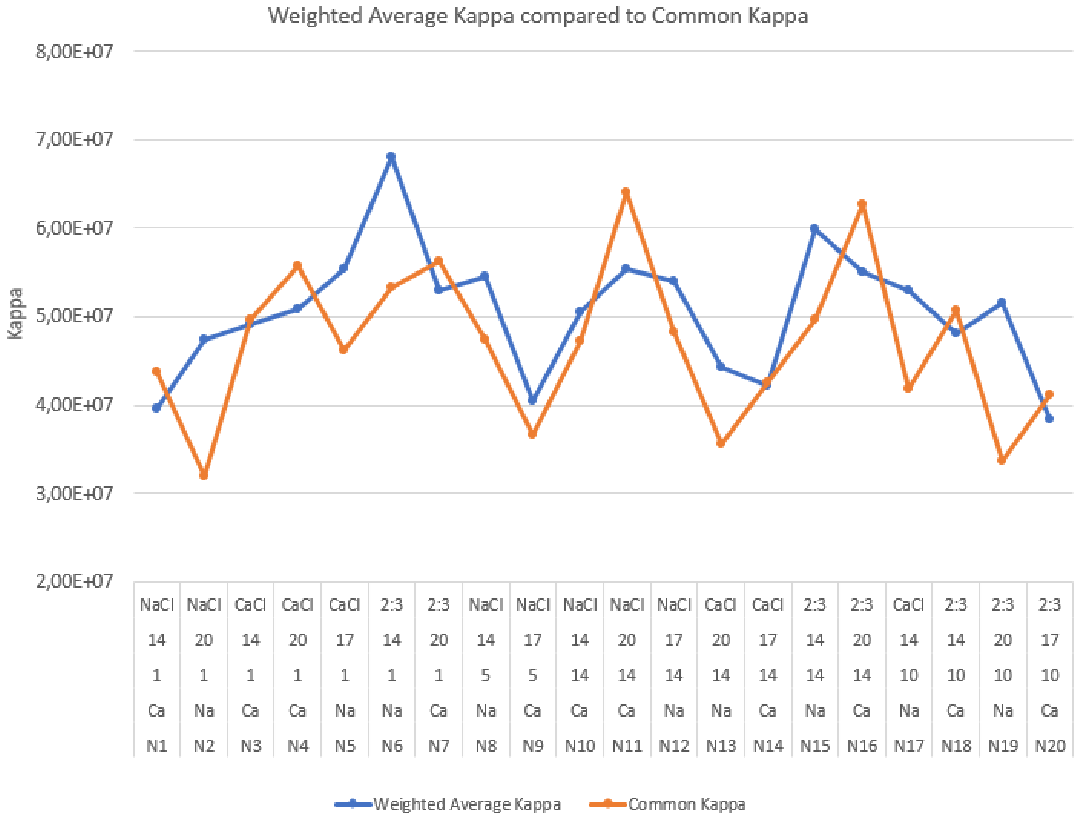

Figure 23: A visual comparison of the obtained kappa values from the two approaches. The DoE conditions for each sample are listed below each sample point. The order of the DoE conditions from bottom to top is Sample number, Bentonite Type, Waiting Time, Water Content, and Water Salinity.

The above table and figure reveal the difference in the kappa values based on the method used to obtain them. Some kappa values are almost identical, for instance, CC_N3 and CC_N14; however, some values have a significant difference, such as CC_N2 and CC_N19. The reason for this difference seems to be the bentonite type. Calcium bentonite causes a smaller difference between the kappa values obtained than sodium bentonite. This is confirmed by taking the ten samples with the smallest difference, where nine out of these ten samples have calcium bentonite as their bentonite type.

To further understand which kappa value is more accurate, **Figures 24** and **25** show both fitted functions plotted against the calibrated loading data. Once again, CC-N4 and CC-N8 are used.

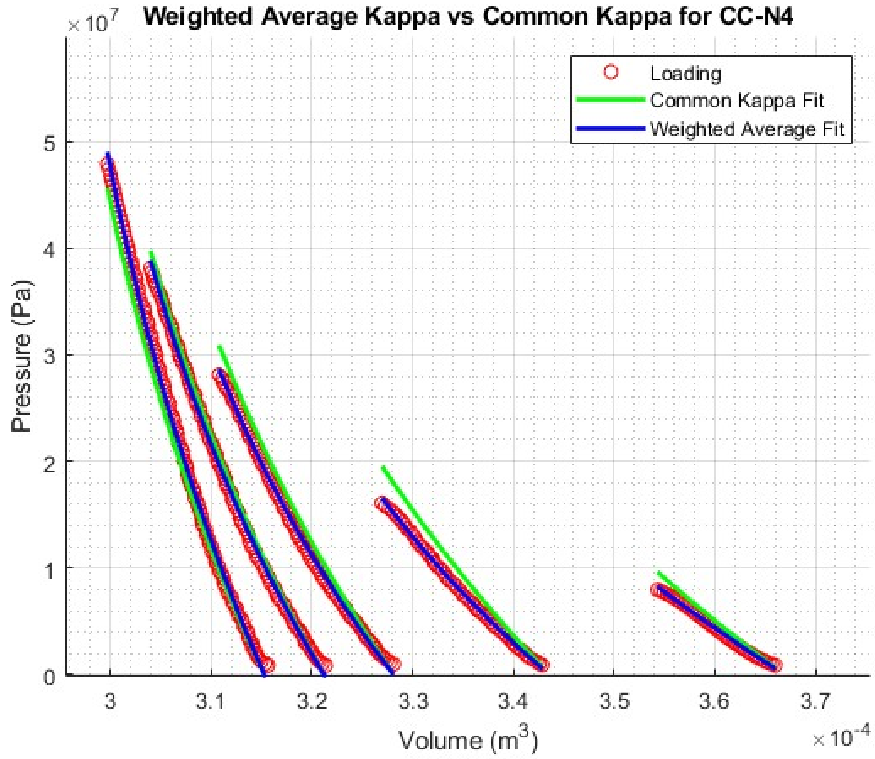

Figure 24: Elastic fit comparison plot for CC-N4.

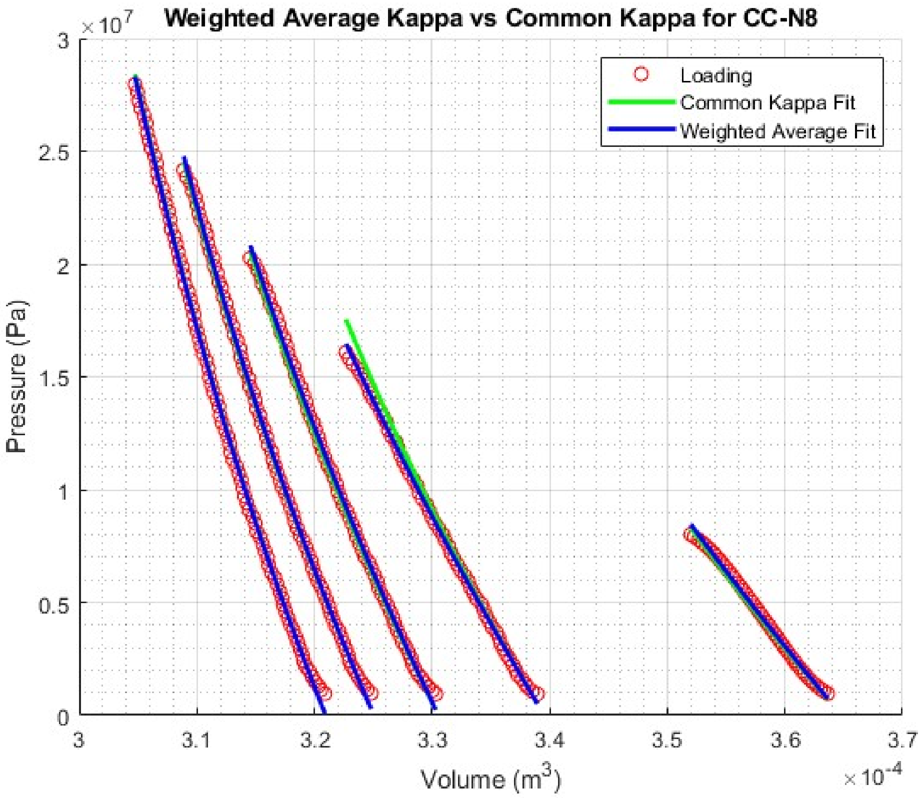

Figure 25: Elastic fit comparison plot for CC-N8.

As can be observed from the figures above, both kappa values give decently good fits for the elastic loading phases. It can also be observed that the more accurate fit is the weighted average kappa method. Therefore, the weighted average kappa-values are used when further developing the surrogate model for the elastic stages.

4.2.2 Lambda Values

The plastic lambda values (λ) were obtained by fitting the mentioned function in the literature review, equation 2.29, to the plastic deformation points of the calibrated data. Fitting the plastic Lambda Values was more straightforward than fitting the Kappa values. Only one approach was used for the lambda values, and thus, only one lambda value was obtained for each experiment. The function was fitted from the plastic deformation point. The Lambda values obtained can be seen in **Figure 26**.

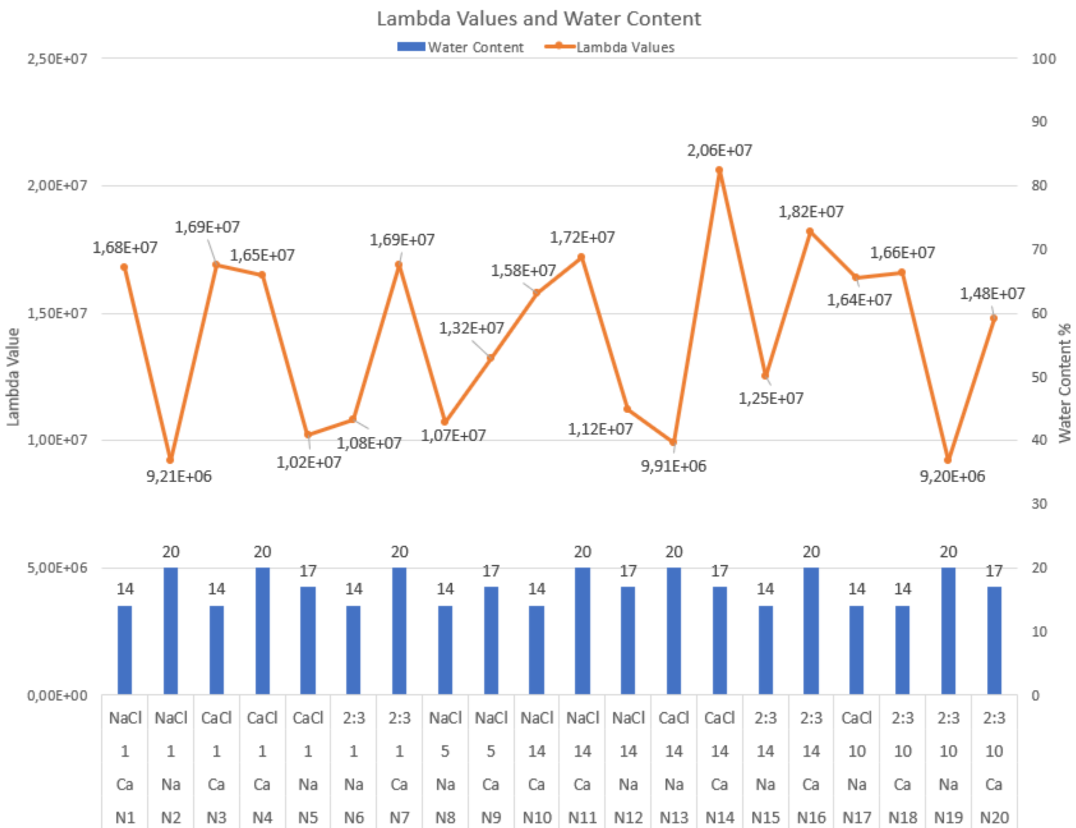

Figure 26: The Lambda-values obtained from the plastic fitting with the water content listed as the blue staples. The DoE conditions are listed below in the order from bottom to top as: Sample Number, Bentonite Type, Waiting Time, and Water Salinity.

The plastic deformation fit for CC-N4 and CC-N8 is shown in **Figures 27** & **28**.

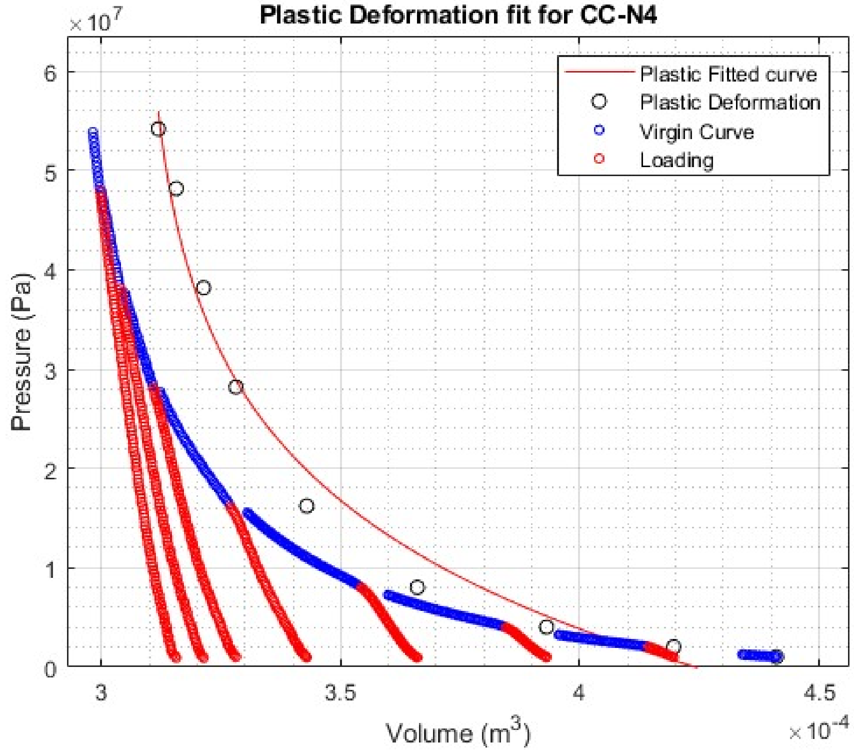

Figure 27: The plastic fitted curve for CC-N4.

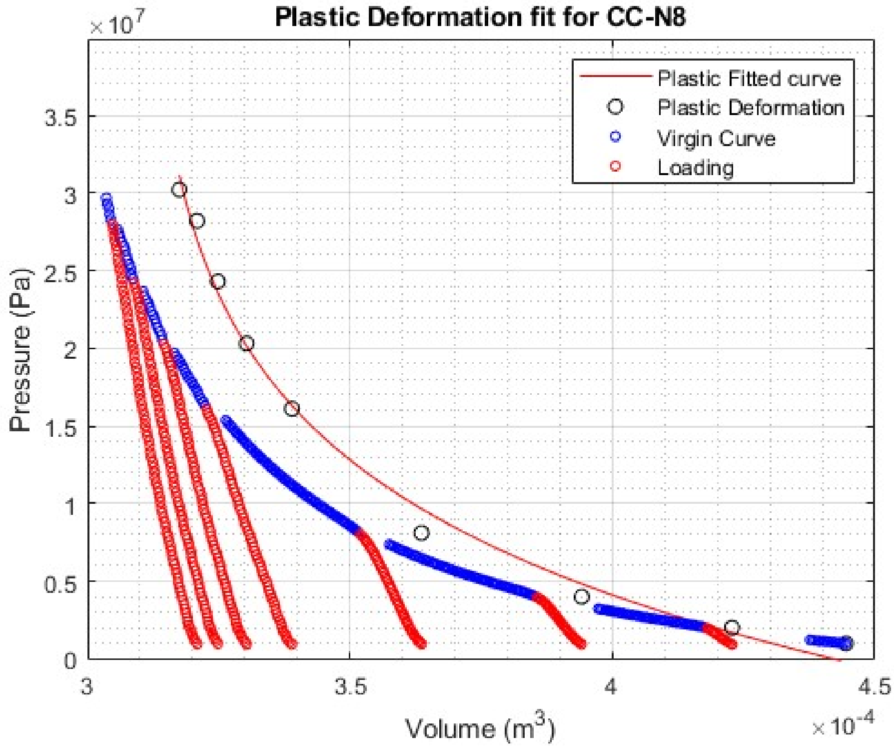

Figure 28: The plastic fitted curve for CC-N8.

As can be observed from the figures above, the fitted plastic function is accurate enough and therefore usable when developing the plastic surrogate model. The low number of plastic deformation points facilitates the process of obtaining the lambda values but increases the uncertainty. The elastic and plastic surrogate models are further developed and presented in the following chapter.

4.3 Surrogate Models

The kappa values characterize the elastic behaviour of the bentonite under pressure during the elastic loading phase. The magnitude of the values reflects the bentonite's resistance to withstand volume reduction under pressure. Therefore, a higher kappa value for the bentonite sample indicates that the sample is less compressible and requires a higher pressure to achieve volume reduction. On the contrary, a low kappa value indicates that the bentonite samples have greater compressibility, meaning the sample can achieve significant volume reduction with less applied pressure.

Similarly, the lambda values characterize the plastic strain-hardening behaviour of the bentonite under pressure. The lambda value's magnitude reflects the extent of plastic deformation the bentonite samples undergo under pressure. Therefore, high lambda values mean the samples are more resistant to plastic deformation, and the sample is more rigid. Low lambda values indicate that the samples are more susceptible to plastic deformation and, therefore, more ductile.

4.3.1 Elastic Surrogate Model

The kappa values obtained from the model fitting were used as input values for developing the elastic surrogate model. The MODDE software used to develop the surrogate models provides a summary of the fit, explaining the model's validity and reproducibility. MODDE provides two key indicators, R2 and Q2. R2 calculates the model's validity and significance. An R2 value below 0.5 indicates a low significance. The Q2 value calculates an estimate of future prediction precision. A Q2 value greater than 0.5 is warranted (Sartorius, 2017). The R2 and Q2 values for the elastic surrogate model were 0.988 and 0.902, respectively, which indicates that the model is valid and reproducible.

MODDE also calculates a coefficient plot showing the significance of the terms in the model. If the term has a considerable distance from y=0 in either direction, the term is deemed to be significant to the model. A non-significant term is a term with a distance close to y=0 (Sartorius, 2017). **Figure 29** shows the coefficients for the elastic surrogate model and their significance.

Non-significant terms were removed to ensure only significant terms were included.

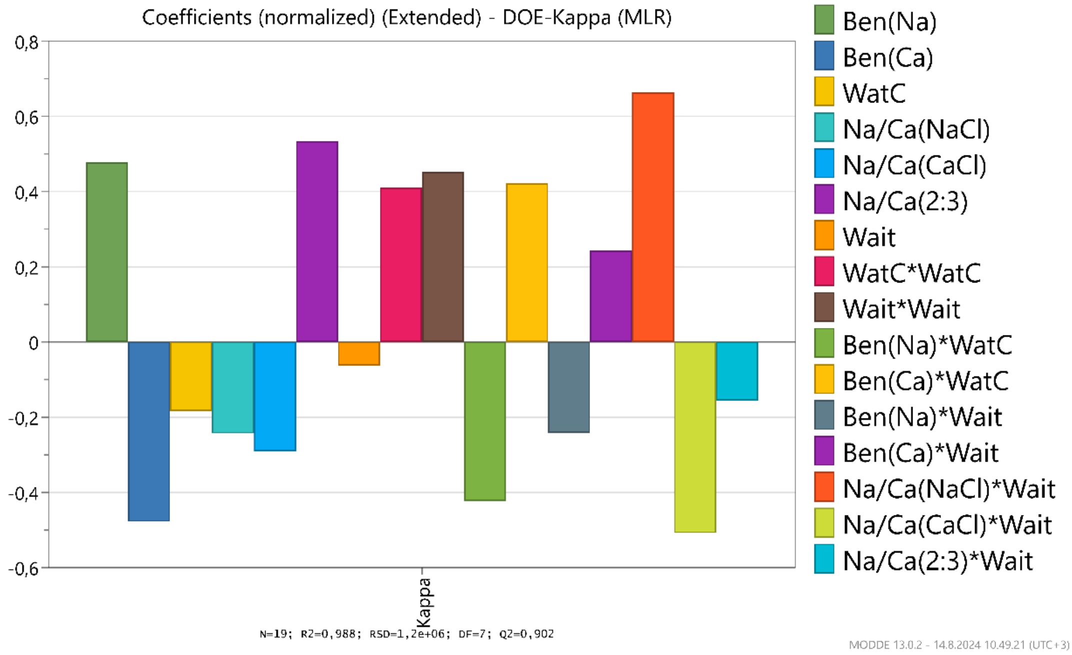

Figure 29: The coefficient plot for the elastic surrogate model, where interaction terms were removed: Bentonite Type and Water salinity, Water content and Water Salinity, and Water content and Waiting time.

It is essential to examine the first-order terms at the beginning and determine their significance. If the first-order terms are significant, the second-other terms involving them are examined. However, if the first-order term is insignificant, the second-order term involving them can be neglected. In this thesis, there is a total of 7 first-order terms. The two different bentonite types and the water salinity mix are the three most significant first-order terms. It can be assumed that depending on the bentonite type used, sodium bentonite will generate higher kappa values, making sodium less susceptible to elastic deformations. On the contrary, calcium bentonite will give, in general, lower kappa values and, therefore, make the samples more prone to elastic deformations. Similarly, the 2:3 water salinity mix will also generate higher kappa values making the samples mixed with that water salinity harder to compress. The other two water salinities, NaCl and CaCl, make the bentonite samples more prone to elastic deformations, where lower kappa values will be generated when either of these salinities is used.

Another finding based on the coefficients is that the water content is not too significant in the regression model, even though it greatly influences how well bentonite can be compacted. This means that the fitted constitutive model that was used to obtain the kappa values seems to take the water content into account relatively well. This suggests that the influence of water content is incorporated into the used measure for strain that considers large deformations and porosity. However, the square term of water content is rather significant. This indicates that there is a nonlinear effect between the independent water content and the dependent kappa value. Therefore, it can be assumed that the effect of water is not too significant in itself at these levels, but once the water content goes beyond these levels, the impact of water content sharply increases.

The same thing can be said about the impact of waiting time. The first-order term of waiting time is the least significant term out of all, meaning that it does not affect the kappa values at all and is, therefore, negligible. However, the square term of the waiting time is greater and, therefore, significant. Therefore, the conclusion about waiting time can be drawn as that 14 days were too short to notice any determinable impact on the elastic behaviour of the bentonite samples, but if the waiting time was to be increased, a significant impact on the elastic behaviour could be noticed due to the large square term of waiting time. After examining the relevant terms, a factor comparison between the first-order terms is conducted like a spider graph shown in **Figure 30**.

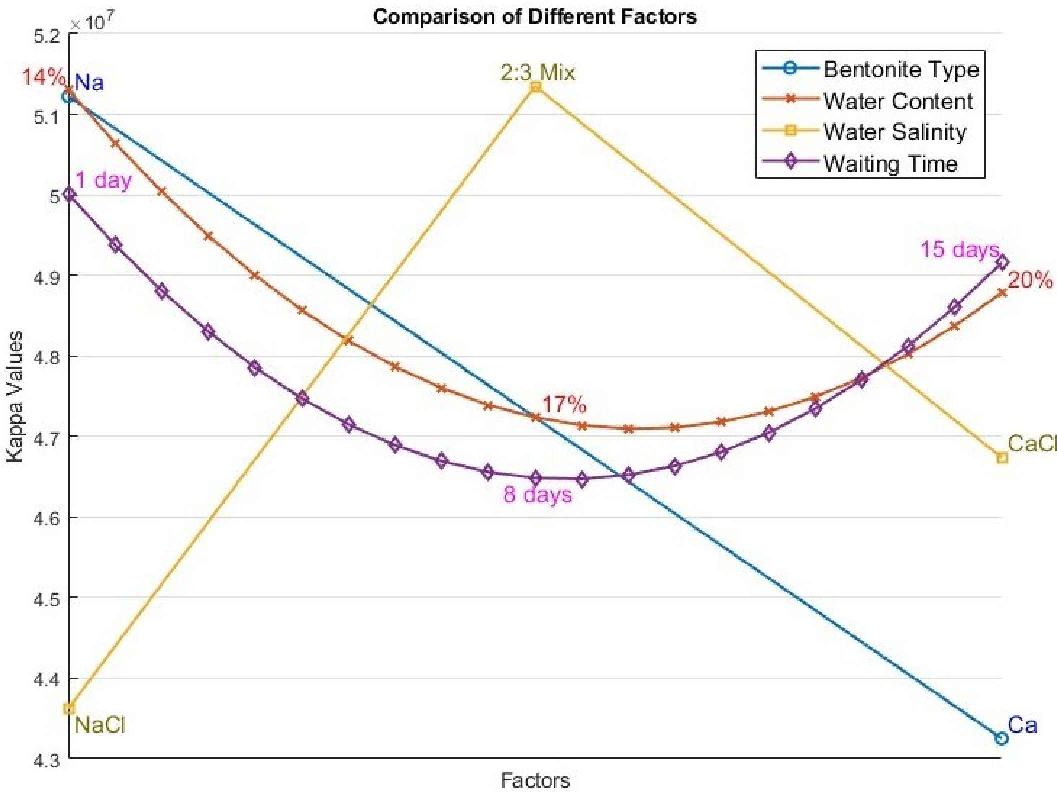

Figure 30: Factor effects for the kappa values for each of the four factors included in the DoE.

The above spider graph confirms the conclusions drawn from the coefficient plot. There is a significant difference between the kappa values generated depending on the bentonite type used. Sodium bentonite will generate higher kappa values overall than calcium bentonite. Additionally, the water salinity 2:3 mix generates higher values than the two other salinities. The square terms that indicate nonlinear behaviour can also be identified for both the waiting time and water content.

After examining the significant terms and the spider graph, contour plots for each possible sample configuration are computed in the MODDE software. **Figures 31** to **33** show the elastic surrogate models for sodium bentonite and calcium bentonite as contour plots. The three different water salinity alternatives are presented in the order NaCl, CaCl, and lastly, the 2:3 combination. The same contour scale is used for all figures to clarify the differences between the bentonite types.

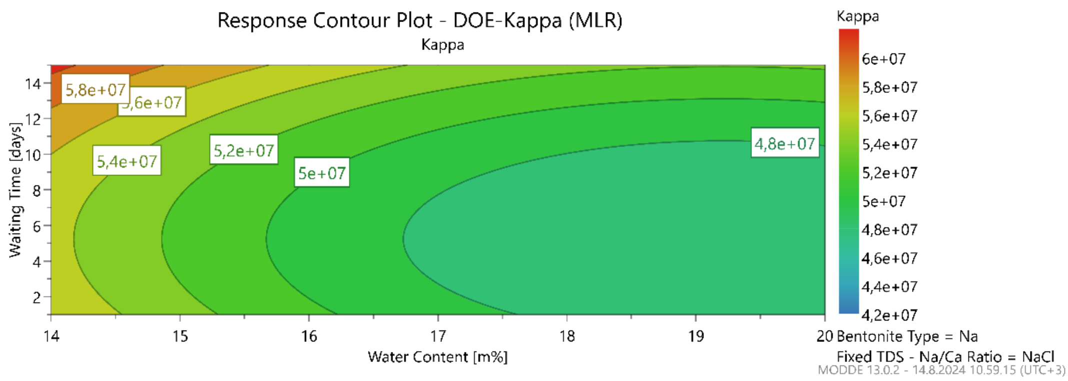

Figure 31: The elastic surrogate model for sodium bentonite and NaCl water salinity with water content on the X-axis and waiting time on the Y-axis.

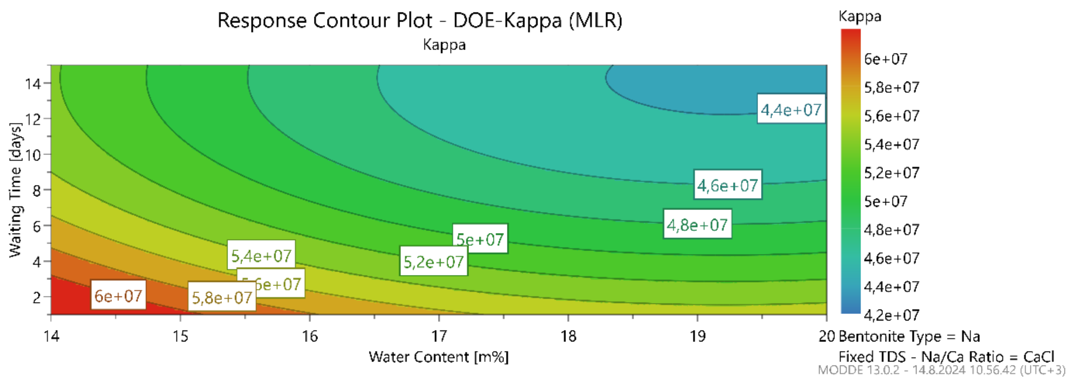

Figure 32: The elastic surrogate model for sodium bentonite and CaCl water salinity.

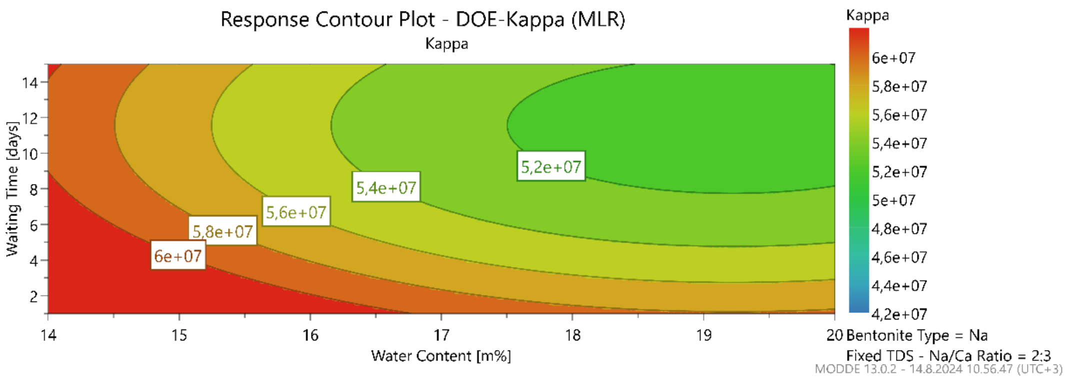

Figure 33: The elastic surrogate model for sodium bentonite and 2:3 water salinity.

As shown in the figures above, the compressibility of sodium bentonite changes depending on the water salinity used. In the first contour plot, with NaCl as the water salinity, a shorter waiting time decreases the kappa value. This means waiting time, in this instance, makes the sodium bentonite less compliant to volume change as time goes on. Additionally, with NaCl as the water salinity, lower water content leads to higher kappa values, resulting in greater resistance towards volumetric change. In the second plot, with CaCl as the water salinity, the waiting time has the opposite effect. The highest kappa values can be obtained after the shortest waiting time at the lowest water content, which makes samples located in that area the most resistant towards volume change. The lowest kappa values are seen at the longest waiting time and highest water content, which makes these samples most prone to elastic deformations. The third contour plot, with the 2:3 mixture as the water salinity, follows the same pattern as the second contour plot but has higher kappa values, indicating poorer compressibility than the CaCl samples in the second plot.

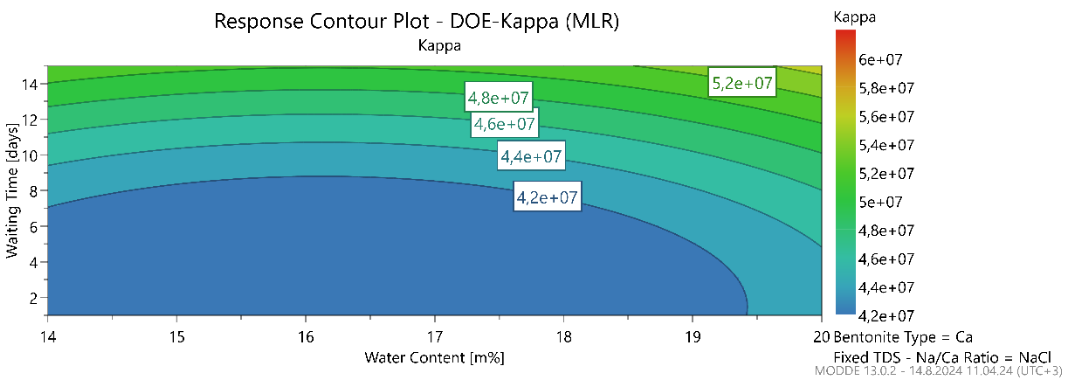

Figure 34: The elastic surrogate model for calcium bentonite and NaCl water salinity with water content on the X-axis and waiting time on the Y-axis.

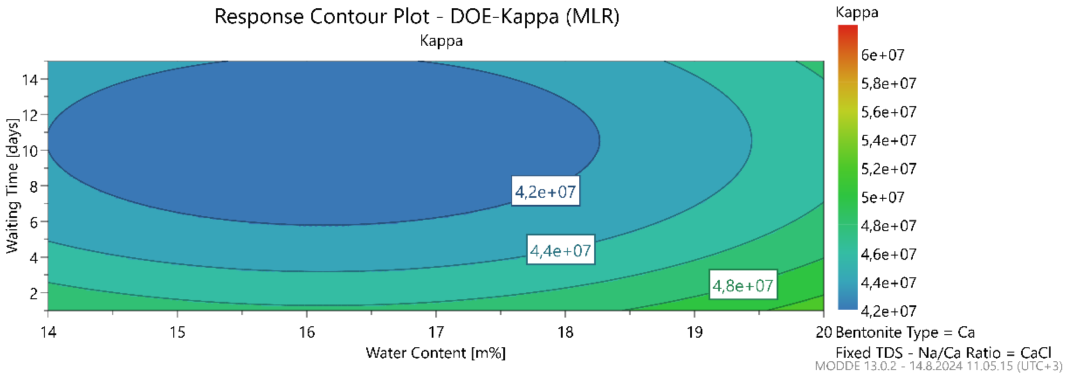

Figure 35: The elastic surrogate model for calcium bentonite and CaCl water salinity.

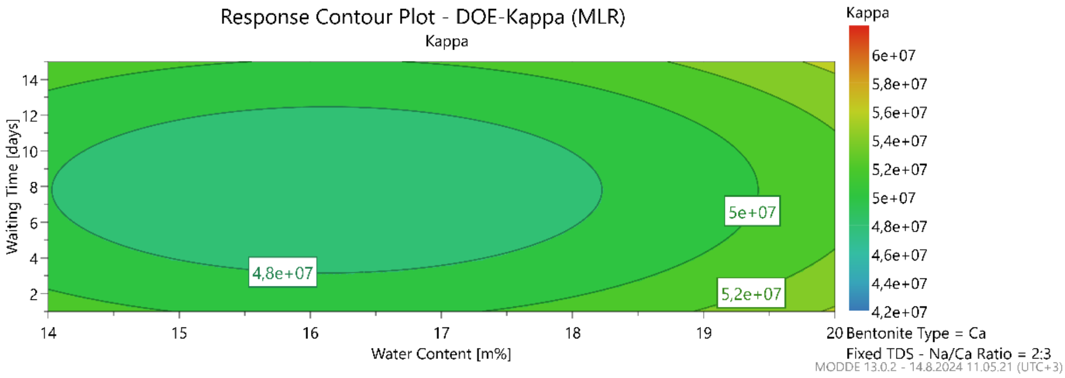

Figure 36: The elastic surrogate model for calcium bentonite and 2:3 water salinity.

For calcium bentonite, the first contour plot with NaCl as the water salinity shows the lowest kappa values for any of the six configurations. The lowest kappa values are obtained with a short waiting time and a low to middle level of water content. With increased waiting time, the kappa values increased, making the bentonite less compressible. Increased water content also influences compressibility, making the kappa values slightly higher. In the second contour plot, with CaCl as the water salinity, the lowest kappa values are observed after the longest waiting time with low to middle water content. The kappa values slightly increase with a shorter waiting time and higher water content. In the third contour plot, with the 2:3 mixture, the kappa values are significantly higher than for the first two plots, indicating that this configuration is less prone to elastic deformations. The Modde software also illustrates the surrogate models as surface plots. **Figure 37** shows the surface plot for sodium bentonite and NaCl water salinity.

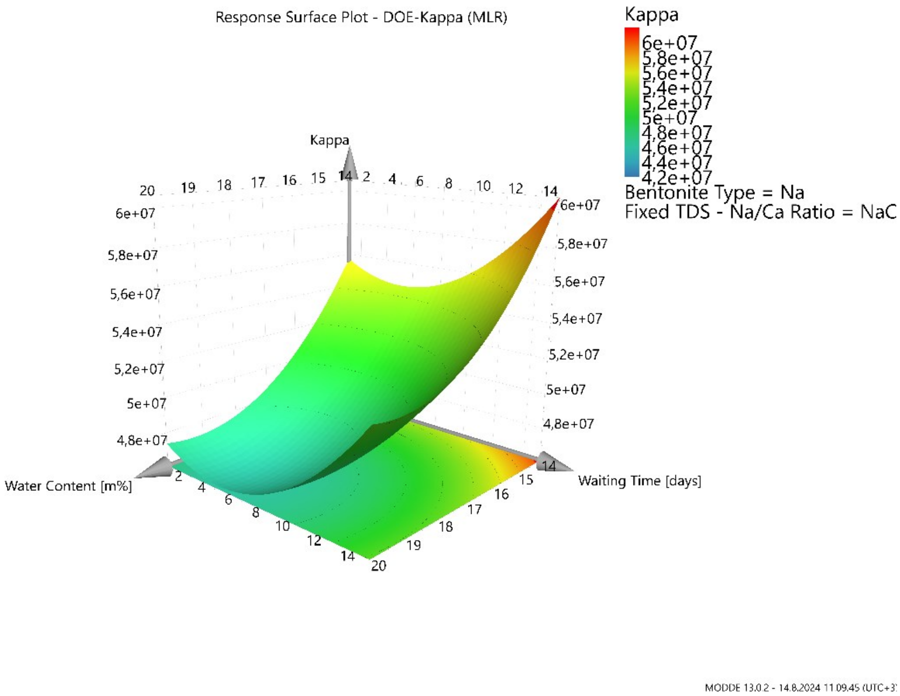

Figure 37: The surface plot for sodium bentonite and NaCl water salinity shown with an identical contour scale.

The other surface plots are not shown but follow the same format. As described earlier in this chapter, the water content and waiting time do not have a significant role in the elastic surrogate model. Therefore, when examining the contour plots, it is more important to compare the different values between bentonite types and water salinities as the first-order terms of these factors in the regression model are more significant. As can be seen in the contour plots, there is a notable difference between the bentonite types. Sodium bentonite generates higher kappa values than calcium bentonite does. The reason for this difference is that the physical and chemical properties of both types are different. For example, the grain size of the calcium bentonite was coarser than that of sodium bentonite, which means the initial porosity of the calcium bentonite is likely higher and, therefore, more compressible.

One aspect that could have affected the calcium bentonite elastic surrogate model was the variability in achieved dry densities. The average dry density for the sodium bentonite samples was 1649 kg/m3, while the average dry density for the calcium bentonite samples was 1587 kg/m^3. The difficulty in achieving high dry densities for calcium bentonite samples might have skewed the elastic surrogate model. However, the lower final dry density of calcium bentonite only means lacking data points at high dry densities which likely makes the effect small. By examining the surrogate model, the effect of bentonite type, water salinity, water content, and waiting time can be more easily understood and used when optimizing the bentonite barrier for the final disposal concept, especially in the elastic stages when precise control of material compressibility and reversibility is required.

4.3.2 Validation of Elastic Surrogate Model Accuracy

As there are several ways of obtaining the kappa values to develop the elastic surrogate model, a way of validating the results is needed. A new way of obtaining the kappa values was introduced to validate the model's accuracy. The kappa values were obtained by taking the individual kappa values for the last two loading phases and taking the average value from those two phases. After that, a similar analysis in Modde was conducted. **Figure 38** shows a spider graph similar to the one shown earlier.

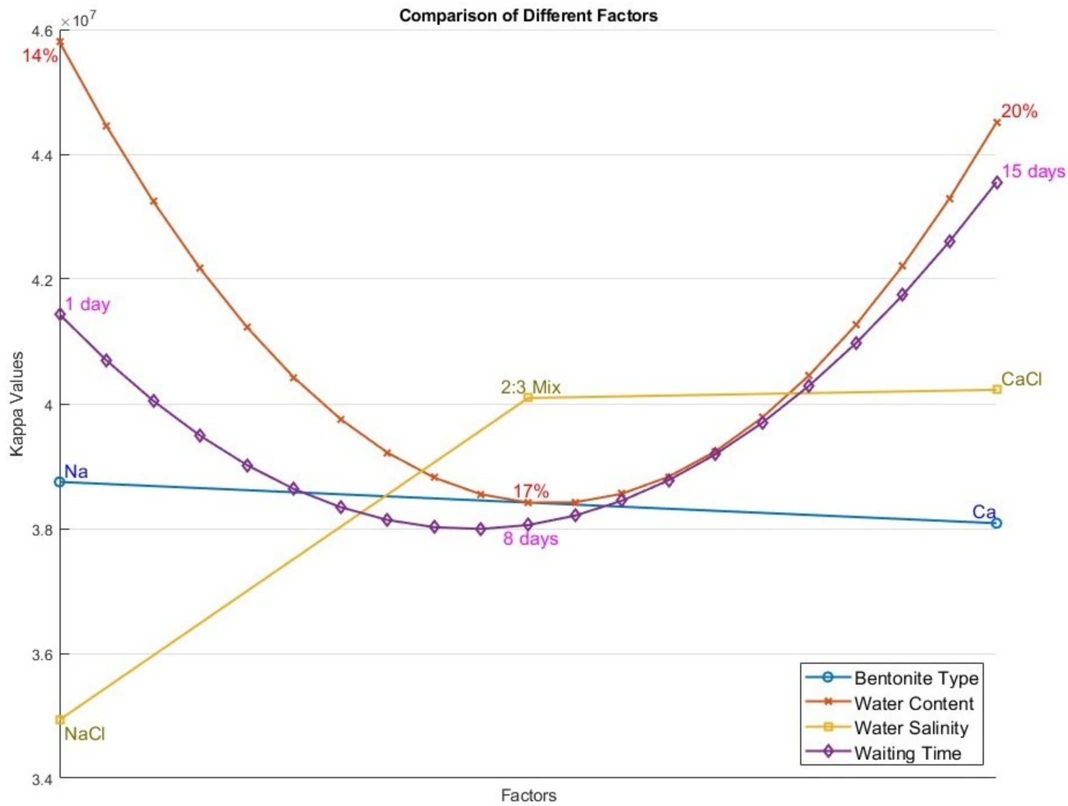

Figure 38: The spider graph from kappa values obtained by taking the average individual kappa value from the last two loading phases.

As can be seen from the above figure, similar tendencies for all four first-order terms can be confirmed. The difference is not as significant for the bentonite type. This is because the last two loading phases for both bentonite types are pretty similar, while a more significant difference is seen in the earlier loading phases between the two types. As the initial loading phases are neglected from the model, the difference between the bentonite types is not as significant. The water salinities follow the same pattern also, which validates the initial results. Again, the water content and waiting time are not too significant, but the same non-linear tendencies can be spotted in the spider graph.

Even though this validates the initial elastic surrogate model results, this model is not as accurate because the initial loading phases are not considered. The initial model includes all loading phases and better captures the differences between the first-order terms. Therefore, the first elastic surrogate model presented should be used for further analysis, and this is only a way of validating the results.

4.3.3 Plastic Surrogate Model

For developing the plastic surrogate model, the lambda values were used the same way as the kappa values for the elastic model. The R2 value in this case was 0.997, and the Q2 value was 0.874, which makes this model both valid and reproducible. The most influential first-order term, seen in **Figure 39**, is primarily the bentonite type.

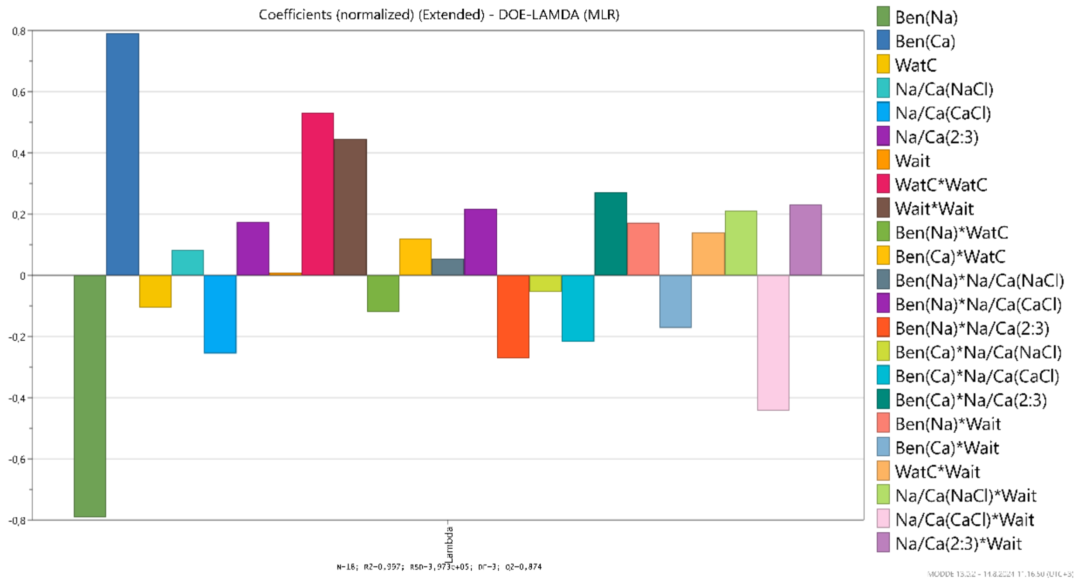

Figure 39: The coefficient plot for the plastic surrogate model. This plot removes the interaction term between water content and water salinity.

Similarly to the elastic surrogate model, the first-order term of bentonite type has the most significant role in the plastic surrogate model. However, when dealing with plastic deformations, the bentonite types have the opposite effect compared to elastic deformations. According to the plastic coefficient plot, sodium bentonite configurations will generate lower plastic lambda values than calcium bentonite. Therefore, sodium bentonite is more prone to plastic deformations than calcium bentonite.

Also, similar to the elastic surrogate model, water content and waiting time have no significant impact. A low significance in the water content means that the fitted constitutive model is also able to take the water content into account quite well during the plastic deformations. However, a significant square term for water content indicates a nonlinear relationship between the water content and the lambda value. Additionally, waiting time had almost no impact at all, but the larger square term indicates that with a longer waiting time, there might be an increase in influence. Out of the three different water salinities, CaCl had the most significant impact by generating lower lambda values, making it more prone to plastic deformations, and the other two salinities had the opposite effect. The factor comparison for the lambda values is drawn in the same way as for the kappa values in **Figure 40**.

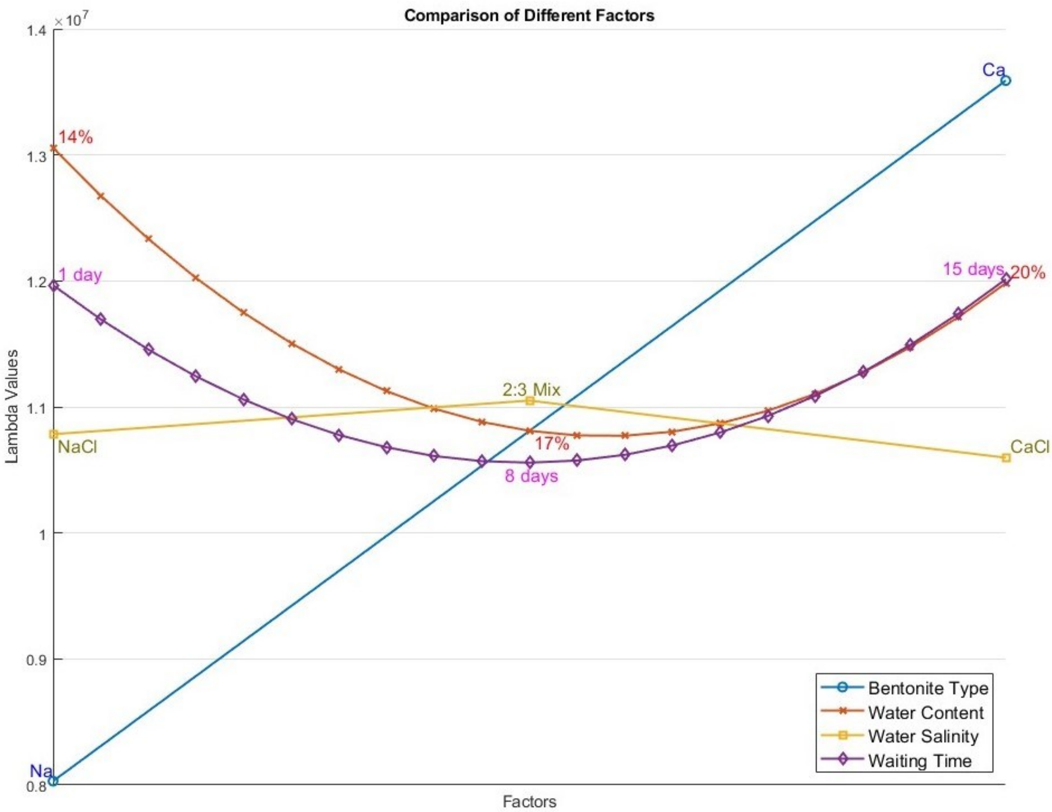

Figure 40: Factor effects for the lambda values for each of the four factors included in the DoE.

The bentonite type is the most significant factor for the lambda values, and this is confirmed by the spider plot. However, unlike the kappa values, calcium bentonite will generate higher lambda values overall than sodium bentonite. Water salinity is an impactful factor but not as relevant as for the kappa values. Also, the water content and waiting time have a less significant role, but their nonlinear tendencies can be spotted in the spider graph.

The plastic surrogate models are presented in the same way as the elastic model with sodium bentonite presented in **Figures 41** to **43** with water salinity order as NaCl, CaCl, and 2:3 mixture. **Figures 44** to **46** show the calcium bentonite model where the water salinity order remains unchanged. The same contour scale is used for all six figures.

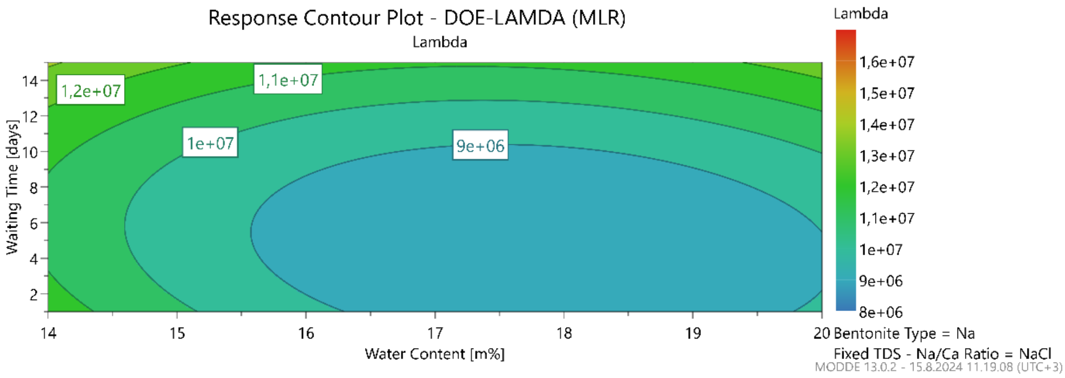

Figure 41: The plastic surrogate model for sodium bentonite and NaCl water salinity with water content on the X-axis and waiting time on the Y-axis.

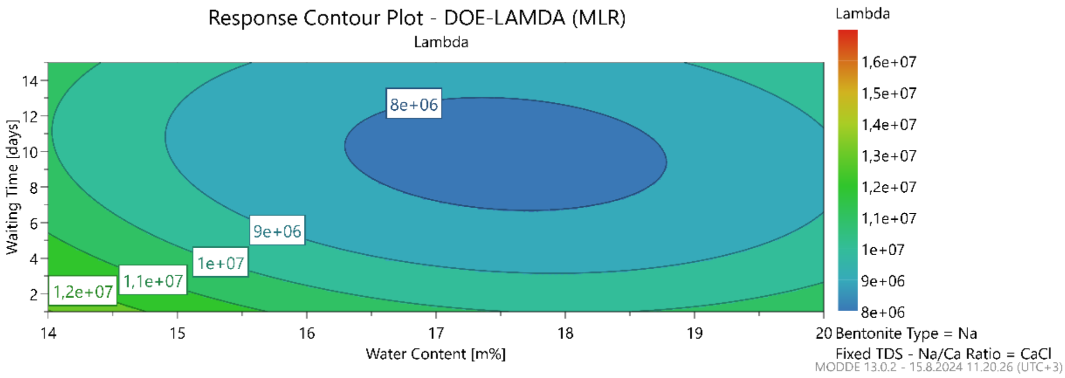

Figure 42: The plastic surrogate model for sodium bentonite and CaCl water salinity.

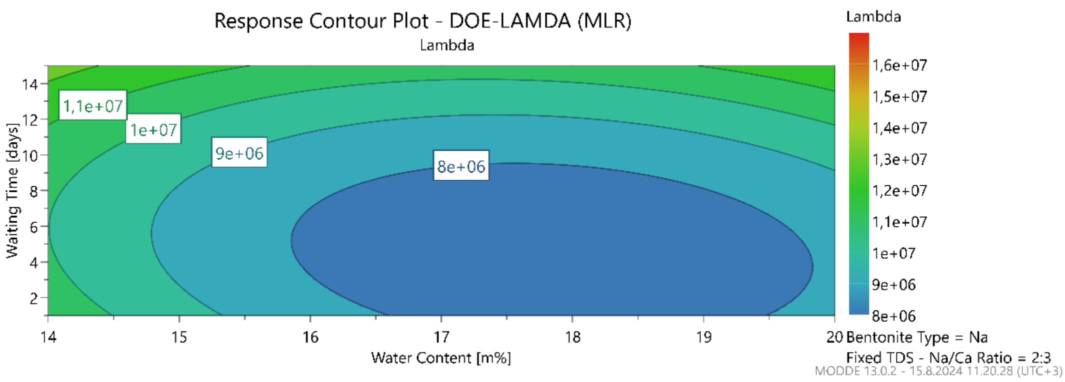

Figure 43: The plastic surrogate model for sodium bentonite and 2:3 water salinity.

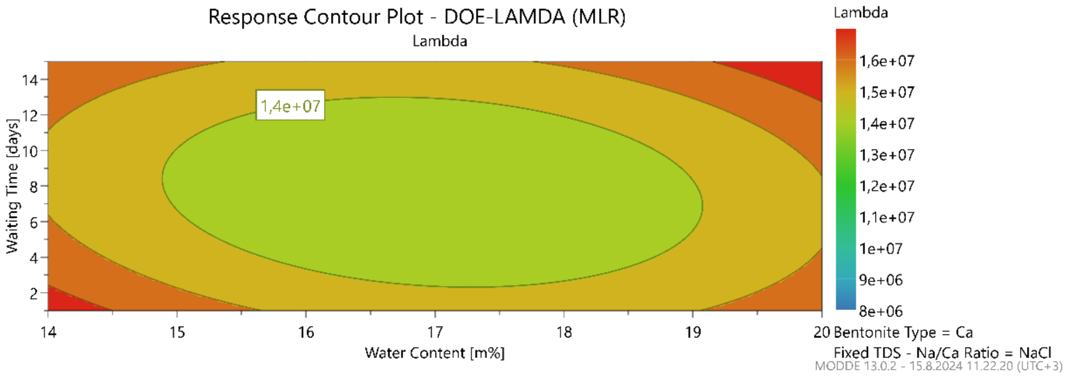

Figure 44: The plastic surrogate model for calcium bentonite and NaCl water salinity.

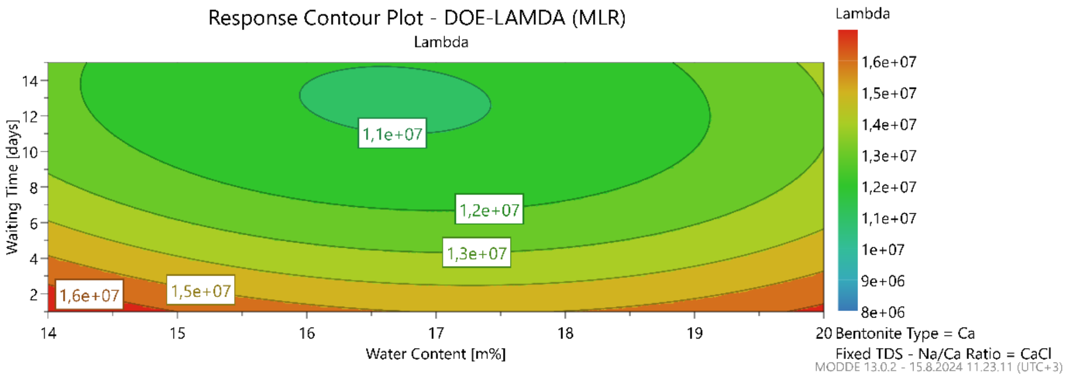

Figure 45: The plastic surrogate model for calcium bentonite and CaCl water salinity.

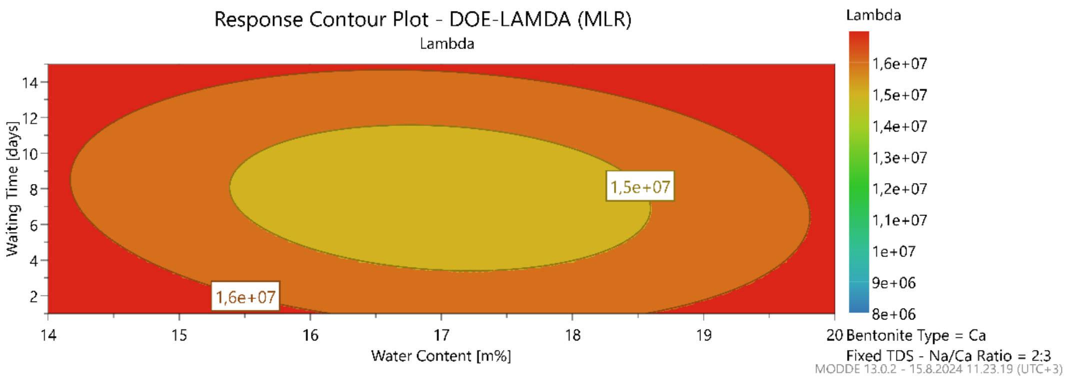

Figure 46: The plastic surrogate model for calcium bentonite and 2:3 water salinity.

As can be observed from **Figures 41** to **43** examining the sodium bentonite, the sodium bentonite obtains the lowest lambda values at middle to high levels of water content for all three water salinities. For NaCl as the water salinity, increased waiting time increases the lambda value, making it less prone to plastic changes under pressure. The second contour plot, with CaCl as the water salinity, is very similar to the first contour plot and obtains similar lambda values. The third contour plot follows the same pattern as the first, with the lowest lambda values at middle to high water content levels and short waiting times. In the third contour plot, with sodium bentonite and the 2:3 water mixture, the lambda values increase with an increase in waiting time, making the bentonite more ductile.

In **Figures 44** to **46**, with calcium bentonite, the lambda values are higher overall than those for sodium bentonite. This indicates that the calcium bentonite samples are less compliant towards permanent deformation. **Figures 44** and **46** follow the same pattern, where the lowest lambda values can be seen after a medium-long waiting time and at middle water content. **Figure 45**, with calcium bentonite and CaCl water salinity, is shifting upwards a bit compared to the other calcium bentonite examples, generating lower lambda values over time. This means that the CaCl water salinity reacts with the calcium bentonite, which makes it more prone to plastic deformations. It should also be noted that the inability to achieve the target dry density for the calcium bentonite samples might skew the plastic surrogate model at high pressures.

The difference in lambda values between sodium bentonite and calcium bentonite is also tied to their chemical and physical properties. There are several factors that affect this outcome, such as grain structure and arrangement. To conclude, sodium bentonite shows lower lambda values, reflecting its greater inclination toward permanent deformation. On the other hand, the higher lambda values obtained for the calcium bentonite demonstrate its lesser tendency towards plastic deformation. While the bentonite type impacts the plastic compaction behaviour most significantly, water content, water salinity, waiting time, and a combination of all four factors influence and differentiate between the plastic surrogate models developed. These differences are critical to understanding when predicting the behaviour of different bentonite configurations in the final disposal concept, especially in a concept where plastic deformations are a crucial consideration.

5 Conclusions

Bentonite is a critical material used as a natural swelling barrier in the final disposal concept for nuclear waste in Finland. This thesis aimed to develop experimentally based surrogate models for predicting the elastic and plastic volumetric compression behaviour of partially saturated bentonite clay. In the research, background research, literature review, development of a new compaction station, extensive mechanical testing, and advanced data analysis were conducted and included. Finally, elastic and plastic surrogate models were developed and examined.

This thesis started with a detailed literature review to understand the current state of the bentonite barriers in the final disposal concept. A quick look at the performance targets and design requirements was followed up with an examination of the different loads acting on the bentonite barrier, the buffer design parameters, and the buffer production process. Afterwards, isotropic volumetric compaction was introduced, and a quick examination of elasto-plastic modelling was performed.

The new compaction station was then planned, built, and tested to address the limitations of the old one. The new station allows for more accurate and reliable testing of bentonite samples. De-aerated water is a less messy fluid than silicon oil, and the new compaction station can reach pressures up to 100MPa.

A carefully drafted DoE plan was then developed, and mechanical testing was performed according to the DoE. The DoE systematically examined variations for different factors: bentonite type, water content, water salinity, and waiting time. In total, 20 different configurations were tested. Data from each experiment was collected, analysed, and used to develop surrogate models in MODDE software. The surrogate models provided insights into the samples' elastic and plastic compression behaviour.

Elastic surrogate model conclusion:

- The elastic surrogate model was highly valid and reproducible with R2 and Q2 values of 0.988 and 0.902.
- Bentonite type is the most significant term when determining the elastic response for a bentonite configuration. Sodium bentonite generates higher kappa values and is less prone to elastic deformations than calcium bentonite. The significant difference in elastic behaviour between the different bentonite types originates from their physical and

chemical properties, such as grain structure and pre-dominant cations.

- The 2:3 water salinity mix generates higher kappa values than the two other salinities. This could be because the salinity mix creates a more stable bentonite structure, making it harder to compress.
- Water content does not significantly impact the elastic surrogate model, although it affects the bentonite behaviour. It seems that the elastic constitutive model with large deformation strain that considers porosity captures the effect of water content well. The square term of water content is, however, significant, and therefore, a nonlinear relationship between the water content and kappa values can be confirmed.
- Waiting time is the least significant first-order term and could be neglected. However, the square term of waiting time is significant, indicating that longer waiting times might impact the model more significantly.
- The different approach to obtaining the kappa values validates the accuracy of the elastic surrogate model.
- The most realistic case is sodium bentonite combined with the 2:3 water mixture, and this model could be used to analyse real-world scenarios.

Plastic surrogate model key findings:

- The plastic surrogate model was highly valid and reproducible with R2 and Q2 values of 0.997 and 0.874.
- Bentonite type had the most significant impact out of any term on the plastic compression behaviour. In contrast to the elastic surrogate model, calcium bentonite generates higher lambda values than sodium bentonite, and calcium bentonite is, therefore, more resistant to plastic deformations.
- Water salinity, water content, and waiting time follow the same conclusions drawn for the elastic surrogate model.

It should be noted that achieving the target dry density for calcium bentonite samples was more challenging than for the sodium bentonite samples, which may have influenced the surrogate models.

This thesis has provided accurate surrogate models for predicting the elastic and plastic volumetric compression behaviour of partially saturated bentonite clay. The surrogate models can be used to optimize the bentonite barriers, which ensures their long-term performance and safety in the final disposal concept.

However, this thesis opens several future research directions. Further studies should investigate an even longer time frame, as the square term of waiting time is significant and could, therefore, impact the waiting time if it were extended. Shear behaviour analysis should also be added to further provide a comprehensive understanding of bentonite's mechanical properties. Additionally, incorporating machine learning and artificial intelligence into the modelling process could enhance the predictive accuracy of the surrogate models.

References

Bell, E., Bryman, A., & Harley, B. (2019). *Business research methods* (Fifth edition. ed.). Oxford University Press.

Davison, L. (2001). *Compression and swelling*. Retrieved 26.3.2024 from https://environment.uwe.ac.uk/geocal/soilmech/compression/soilcomp.htm#COMPRISOEQ

Dueck, A., & Nilsson, U. (2010). *Thermo-Hydro-Mechanical properties of MX-80. Results from advanced laboratory tests* (SKB-TR-10-55). http://www.skb.se/upload/publications/pdf/TR-10-55webb.pdf

EI. (2024). Statistical Review of World Energy. https://www.energyinst.org/statistical-review/resources-and-data-downloads

Haldar, S. K., & Tišljar, J. (2014). Chapter 5 - Sedimentary Rocks. In S. K. Haldar & J. Tišljar (Eds.), *Introduction to Mineralogy and Petrology* (pp. 121-212). Elsevier. https://doi.org/https://doi.org/10.1016/B978-0-12-408133-8.00005-5

Hencky, H. (1928). Uber die Form des Elastizitatsgesetzes bei ideal elastischen Stoffen. *Zeit. Tech. Phys.*, *9*, 215-220.

Horowitz, C. A. (2016). Paris Agreement. *International Legal Materials*, *55*(4), 740-755. https://doi.org/https://doi.org/10.1017/S0020782900004253

IEA. (2023). *Finland 2023 Energy Policy Review*. OECD Publishing. https://doi.org/https://doi.org/10.1787/d435fa51-en

Jiang, P., Zhou, Q., & Shao, X. (2020). *Surrogate Model-Based Engineering Design and Optimization* (1st 2020. ed.). Springer Singapore. https://doi.org/https://dx.doi.org/10.1007/978-981-15-0731-1

Juvankoski, M. (2013). *Buffer design 2012*. http://inis.iaea.org/search/search.aspx?orig_q=RN:45087738

Juvankoski, M., Holt, E., Rantamäki, P., & Oy, P. (2013). Designed Buffer Components for Finnish KBS-3V Concept–14285.

Kontula, A., Vira, J., & Pastina, B. (2021). *Graded Development of Geological Disposal Towards Optimized Solution*. http://inis.iaea.org/search/search.aspx?orig_q=RN:53084512

Landau, L. D., Pitaevskii, L., Kosevich, A. d. M., & Lifshitz, E. M. (2012). *Theory of elasticity: volume 7* (Vol. 7). Elsevier.

Lee, H., Calvin, K., Dasgupta, D., Krinner, G., Mukherji, A., Thorne, P., Trisos, C., Romero, J., Aldunce, P., & Barret, K. (2023). IPCC, 2023: Climate Change 2023: Synthesis Report, Summary for Policymakers. Contribution of Working Groups I, II and III to the Sixth Assessment Report of the Intergovernmental Panel on Climate Change [Core Writing Team, H. Lee and J. Romero (eds.)]. IPCC, Geneva, Switzerland. https://doi.org/https://doi.org/10.59327/IPCC/AR6-9789291691647.001

Lubliner, J. (2008). *Plasticity theory*. Courier Corporation.

Merriam-Webster. (2024). Elastoplastic. In *Merriam-Webster.com Dictionary*. Retrieved 12.6.2024, from https://www.merriam-webster.com/dictionary/elastoplastic

Muuri, E. (2021). *Buffer, Backfill and Closure Evolution*. H. Posiva Oy.

Peter Fraser, B. W., Keith Everhart, Antoine Herzog. Luis Lopez, Zoe Hungerford, Max Schoenfisch, Yunyou Chen (2022). *Nuclear Power and Secure Energy Transitions From today's challenges to tomorrow's clean energy systems*. OECD Publishing. https://doi.org/https://doi.org/10.1787/aca1d7ee-en

Posiva Oy, H. (2013). *Safety case for the disposal of spent nuclear fuel at Olkiluoto Models and data for the repository system 2012 Parts 1 and 2*. http://inis.iaea.org/search/search.aspx?orig_q=RN:45087751

Posiva Oy, H. (2016a). *KBS-3H - Design, Production and Initial State of Buffer and Filling Components*.

Posiva Oy, H. (2016b). *Safety Evaluation for a KBS-3H Spent Nuclear Fuel Reporistory at Olkiluoto - Design Basis*.

Posiva Oy, H. (2021a). *Safety Case for the Operating Licence Application - Models and Data (M&D)*. https://cms.posiva.fi/

Posiva Oy, H. (2021b). *Safety Case for the Operating Licence Application - Performance Assessment and Formulation of Scenarios (PAFOS)*. https://cms.posiva.fi/

Pulkkanen, V.-M. (2019). *A large deformation model for chemoelastic porous media : bentonite clay in spent nuclear fuel disposal* Aalto University]. Helsinki. http://urn.fi/URN:ISBN:978-952-60-8372-8

Puzrin, A. (2012). *Constitutive modelling in geomechanics: introduction*. Springer Science & Business Media. https://doi.org/https://doi.org/10.1007/978-3-642-27395-7

Razavi, S., Tolson, B. A., & Burn, D. H. (2012). Review of surrogate modeling in water resources. *Water Resources Research*, *48*(7). https://doi.org/https://doi.org/10.1029/2011WR011527

Rotz, R. (2021). Hydrogeologic properties of earth materials and principles of groundwater flow. In: Wiley Online Library.

Saarela, O. (2024, 22.4.2024). *WHY Design Of Experiments ?* [Interview]. Espoo, Finland;

Sartorius. (2017). *MODDE® 12 User Guide*. In https://www.sartorius.com/download/544636/modde-12-user-guide-en-b-00090-sartorius-data.pdf

Sawicki, A., & Swidzinski, W. (1995). Cyclic compaction of soils, grains and powders. *Powder Technology*, *85*(2), 97-104. https://doi.org/https://doi.org/10.1016/0032-5910(95)03013-Y

Sean, R. (2013). *Part 1 of 3: Introduction to triaxial testing*. https://www.gdsinstruments.com/information/white-paper-introduction-to-triaxial-testing

Vehmas, J., Rentto, A., Luukkanen, J., Auffermann, B., & Kaivo-oja, J. (2023). The Finnish Solution to Final Disposal of Spent Nuclear Fuel. In *The Future of Radioactive Waste Governance: Lessons from Europe* (pp. 287-317). Springer Fachmedien Wiesbaden Wiesbaden.

https://doi.org/https://doi.org/10.1007/978-3-658-40496-3_11#DOI
Williams, B., & Cremaschi, S. (2021). Novel tool for selecting surrogate modeling techniques for surface approximation. In *Computer aided chemical engineering* (Vol. 50, pp. 451-456). Elsevier. https://doi.org/https://doi.org/10.1016/B978-0-323-88506-5.50071-1
Wood, D. M. (1990). *Soil behaviour and critical state soil mechanics*. Cambridge university press.
Yin, Z.-Y., Hicher, P.-Y., & Jin, Y.-F. (2020a). Elastoplastic Modeling of Soils: From Mohr-Coulomb to SIMSAND. In Z.-Y. Yin, P.-Y. Hicher, & Y.-F. Jin (Eds.), *Practice of Constitutive Modelling for Saturated Soils* (pp. 121-176). Springer Singapore. https://doi.org/10.1007/978-981-15-6307-2_5
Yin, Z.-Y., Hicher, P.-Y., & Jin, Y.-F. (2020b). *Practice of constitutive modelling for saturated soils*. Springer. https://doi.org/https://doi.org/10.1007/978-981-15-6307-2